

MODELING ELF RADIO ATMOSPHERICS GENERATED BY ROCKET TRIGGERED  
LIGHTNING

By

BHARAT SIMHA REDDY KUNDURI

A THESIS PRESENTED TO THE GRADUATE SCHOOL  
OF THE UNIVERSITY OF FLORIDA IN PARTIAL FULFILLMENT  
OF THE REQUIREMENTS FOR THE DEGREE OF  
MASTER OF SCIENCE

UNIVERSITY OF FLORIDA

2010

© 2010 Bharat Simha Reddy Kunduri

To my parents,  
K.P.Reddy and Dr.B.Thirumala Devi

## ACKNOWLEDGMENTS

I would like to express my sincere gratitude and thanks to my advisor Dr. Robert Moore for his guidance and support throughout my graduate studies. I thank him for giving me an opportunity to work with him and for his patience and encouragement throughout this project. This thesis would not have been possible without his meticulous guidance and invaluable advice. I thank Dr. Martin Uman and Dr. Vladimir Rakov for readily agreeing to be on my committee and for their constant support and advice.

I thank all my lab mates for their constant encouragement throughout my stay at the lab. I take this opportunity to thank my friends Dhruv Sharma, Anuj Sisodia and Vishal Narayan who were like my family away from home.

Finally, I am deeply thankful to my parents for supporting me in innumerable ways and being a great source of strength at every stage of my life.

## TABLE OF CONTENTS

	<u>page</u>
ACKNOWLEDGMENTS . . . . .	4
LIST OF FIGURES . . . . .	7
ABSTRACT . . . . .	11
CHAPTER	
1 INTRODUCTION . . . . .	13
1.1 The Lightning Discharge . . . . .	14
1.2 Rocket Triggered Lightning . . . . .	16
1.2.1 Classical Rocket Triggered Lightning . . . . .	16
1.2.2 Altitude Rocket Triggered Lightning . . . . .	17
1.2.3 Current Waveforms . . . . .	18
1.3 Radio Atmospheric . . . . .	19
1.4 Ionosphere . . . . .	21
2 INSTRUMENTATION AND LAYOUT AT MCMURDO STATION ANTARCTICA AND CAMP BLANDING . . . . .	25
2.1 McMurdo Station- Antarctica . . . . .	25
2.1.1 Arrival Heights Area, McMurdo Station . . . . .	27
2.1.2 ELF/VLF Research at McMurdo Station . . . . .	28
2.2 International Center for Lightning Research and Testing at Camp Blanding (ICLRT), Florida . . . . .	31
3 ELF PROPAGATION IN THE EARTH-IONOSPHERE WAVEGUIDE . . . . .	37
3.1 Wave Propagation in an Ideal Parallel Plate Waveguide . . . . .	37
3.2 Wave Propagation in Plasma . . . . .	40
3.2.1 Effect of Collisions . . . . .	42
3.2.2 Effect of Static Magnetic Field . . . . .	42
3.3 Properties of Earth-Ionosphere Waveguide . . . . .	43
3.4 Waveguide Mode Theory-Budden.K.G . . . . .	44
3.4.1 Sources of Waves- The Hertzian Dipole . . . . .	44
3.4.2 Modes in the Waveguide . . . . .	45
3.4.3 Reflection Coefficients in the Earth-Ionosphere waveguide . . . . .	47
3.4.4 Mode Equation . . . . .	48
3.4.5 Correction for the Curved Nature of the Earth-Ionosphere Waveguide . . . . .	50
3.5 Long Wavelength Propagation Capability (LWPC) . . . . .	50
3.5.1 PRESEG . . . . .	51
3.5.2 MODEFNDR . . . . .	51
3.5.3 FASTMC . . . . .	52
3.5.4 Implementation in LWPC . . . . .	52

3.6	Parameters Required to Calculate the Sferic Propagation Model . . . . .	54
3.6.1	Ionospheric Electron Density Profiles . . . . .	55
3.6.2	Current Moment Waveform of a Lightning Strike . . . . .	56
4	MODELING ELF SFERICS . . . . .	58
4.1	Homogeneous Waveguide . . . . .	58
4.2	Inhomogeneous Ground . . . . .	60
4.3	Modeling of ELF sferics Propagating from Camp Blanding to McMurdo Station . . . . .	62
4.3.1	Nighttime Ionosphere With a Valley . . . . .	64
4.3.2	Daytime Ionosphere - Type 1 . . . . .	66
4.3.3	Nighttime Ionosphere Without a Valley . . . . .	69
4.3.4	Daytime Ionosphere - Type 2 . . . . .	74
4.4	Effects of Different Components of Current on the Sferic Waveform . . . . .	78
4.4.1	Effects of Current Components - Different Ionospheres . . . . .	85
5	SUMMARY AND SUGGESTIONS FOR FURTHER WORK . . . . .	88
5.1	Summary . . . . .	88
5.2	Suggestions for Further Work . . . . .	89
5.2.1	Jumps in the amplitude . . . . .	89
5.2.2	Modeling at Lower Frequencies - Below 45Hz . . . . .	89
5.2.3	Modeling Using a more Realistic Inhomogeneous Ionosphere . . . . .	90
5.2.4	Remote Sensing of Ionosphere . . . . .	91
	REFERENCES . . . . .	93
	BIOGRAPHICAL SKETCH . . . . .	96

## LIST OF FIGURES

<u>Figure</u>	<u>page</u>
1-1 Various phases of negative cloud to ground lightning discharge Adapted from Rakov and Uman-2003 . . . . .	14
1-2 Classical Rocket Triggered Lightning (V.A.Rakov "Lightning Discharges Triggered Using Rocket and Wire Technique", J.Geophys.Res.,vol.100,pp.25711-25720,1999	17
1-3 Altitude Rocket Triggered Lightning (V.A.Rakov "Lightning Discharges Triggered Using Rocket and Wire Technique", J.Geophys.Res.,vol.100,pp.25711-25720,1999)	18
1-4 Overall current record of a triggered lightning at camp blanding, florida(D.Wang et al., "Characterization of initial stage of negative rocket triggered lightning", J.Geophys.Res.,vol.104,pg 4213-4222,1999) . . . . .	19
1-5 Time domain waveform of a sferic observed at palmer station (adapted from (Wood, 2004)) . . . . .	21
1-6 Day and Night time electron density profiles for sunspot maximum (solid lines) and sunspot minimum (dashed lines), adapted from Tascione, T.F., Introduction to the Space Environment, 2nd Ed. . . . .	22
2-1 A map of Antarctica indicating Ross Island and McMurdo Station . . . . .	25
2-2 A LandSat Map of Ross Island (source: <a href="http://international.usgs.gov">http://international.usgs.gov</a> ) . . . . .	26
2-3 A picture of McMurdo Station (source: <a href="http://international.usgs.gov">http://international.usgs.gov</a> ) . . . . .	26
2-4 Arrival Heights, McMurdo Station . . . . .	27
2-5 A picture of the VLF receiver at McMurdo Station . . . . .	29
2-6 A picture of the ELF receiver at McMurdo Station . . . . .	29
2-7 A picture of the Racks that hold the data acquisition equipment at McMurdo Station,Photo by Robert Moore . . . . .	30
2-8 Overview of ICLRT at Camp Blanding in 2002, source:(Rakov et al., 2003) . .	31
2-9 Satellite image of ICLRT with some of its major landmarks indicated, adapted from (Howard, 2009) . . . . .	34
2-10 A picture of launch tower, Source:Lightning Lab-University of Florida . . . . .	35
2-11 Picture of launch control trailer, Source:Lightning Lab-University of Florida . . .	35
3-1 Ideal Parallel Plate Waveguide . . . . .	38
3-2 Earth-Ionosphere Waveguide . . . . .	53

3-3	Flow chart showing the execution of LWPC . . . . .	55
3-4	Representative electron density profiles . . . . .	56
3-5	Current vs Time waveform from rocket triggered lightning . . . . .	57
4-1	Representative nighttime ionosphere . . . . .	59
4-2	ELF sferic spectra of homogeneous ground in linear scale . . . . .	59
4-3	ELF sferic spectra of homogeneous ground in decibel scale . . . . .	60
4-4	Comparison of ELF sferic spectra for inhomogeneous and homogeneous ground (distance-2000Km) . . . . .	61
4-5	Comparison of ELF sferic spectra for inhomogeneous and homogeneous ground (distance-2000Km) in decibel scale . . . . .	61
4-6	Propagation Path of the Sferic from Florida to Antarctica (Great Circle) . . . . .	63
4-7	Nighttime ionosphere with a valley . . . . .	64
4-8	Current Waveform employed in calculations . . . . .	65
4-9	LWPC output for nighttime ionosphere with a valley . . . . .	65
4-10	Modeled ELF spectrum in decibel scale (over 1 nanotesla) for nighttime ionosphere with a valley . . . . .	66
4-11	Modeled ELF spectrum in linear scale for nighttime ionosphere with a valley . . . . .	67
4-12	Modeled ELF sferic waveform for nighttime ionosphere with a valley . . . . .	67
4-13	Daytime ionosphere type 1 . . . . .	68
4-14	Current Waveform employed in calculations . . . . .	68
4-15	LWPC output for daytime ionosphere type 1 . . . . .	69
4-16	Modeled ELF spectrum in decibel scale (over 1 nanotesla) for daytime ionosphere type 1 . . . . .	70
4-17	Modeled ELF spectrum in linear scale for daytime ionosphere type 1 . . . . .	70
4-18	Modeled ELF sferic waveform for daytime ionosphere type 1 . . . . .	71
4-19	Nighttime ionosphere without a valley . . . . .	71
4-20	Current Waveform employed in calculations . . . . .	72
4-21	LWPC output for nighttime ionosphere without a valley . . . . .	72

4-22 Modeled ELF spectrum in decibel scale (over 1 nanotesla) for nighttime ionosphere without a valley . . . . .	73
4-23 Modeled ELF spectrum in linear scale for nighttime ionosphere without a valley	73
4-24 Modeled ELF sferic waveform for nighttime ionosphere without a valley . . . . .	74
4-25 Daytime ionosphere type 2 . . . . .	75
4-26 Current Waveform employed in calculations . . . . .	75
4-27 LWPC output for daytime ionosphere type 2 . . . . .	76
4-28 Modeled ELF spectrum in decibel scale (over 1 nanotesla) for daytime ionosphere type 2 . . . . .	76
4-29 Modeled ELF sferic waveform in linear scale for daytime ionosphere type 2 . . . . .	77
4-30 Modeled ELF sferic waveform for daytime ionosphere type 2 . . . . .	77
4-31 Components of the Current Waveform Used . . . . .	78
4-32 ICC Component of the Current Waveform Used . . . . .	79
4-33 Resultant Sferic Waveform Caused due to the ICC Component of Current . . . . .	79
4-34 Return Stroke 1 of the Current Waveform Used . . . . .	80
4-35 Resultant Sferic Waveform Caused due to Return Stroke 1 of Current . . . . .	80
4-36 Return Stroke 2 of the Current Waveform Used . . . . .	81
4-37 Resultant Sferic Waveform Caused due to Return Stroke 2 of Current . . . . .	81
4-38 Return Stroke 3 of the Current Waveform Used . . . . .	82
4-39 Resultant Sferic Waveform Caused due to Return Stroke 3 of Current . . . . .	82
4-40 Return Stroke 4 of the Current Waveform Used . . . . .	83
4-41 Resultant Sferic Waveform Caused due to Return Stroke 4 of Current . . . . .	83
4-42 Return Stroke 5 of the Current Waveform Used . . . . .	84
4-43 Resultant Sferic Waveform Caused due to Return Stroke 5 of Current . . . . .	84
4-44 Sferic Waveform and Different Components-Nighttime Ionosphere With a Valley	85
4-45 Sferic Waveform and Different Components-Daytime Ionosphere type 1 . . . . .	86
4-46 Sferic Waveform and Different Components-Nighttime Ionosphere Without a Valley . . . . .	86

4-47 Sferic Waveform and Different Components-Daytime Ionosphere type 2 . . . . .	87
5-1 Variations in the amplitude of the sferic across the path of propagation . . . . .	89

Abstract of Thesis Presented to the Graduate School  
of the University of Florida in Partial Fulfillment of the  
Requirements for the Degree of Master of Science

MODELING ELF RADIO ATMOSPHERICS GENERATED BY ROCKET TRIGGERED  
LIGHTNING

By

Bharat Simha Reddy Kunduri

August 2010

Chair: Robert Moore

Major: Electrical and Computer Engineering

A lightning strike radiates electromagnetic energy over a wide bandwidth ranging from a few Hz to a few hundred MHz, but a major part of this energy is in the Extremely Low Frequency(ELF) range (i.e, 1-3000 Hz) and Very Low Frequency(VLF) range (i.e, 3-30 KHz). This energy whose spectrum spans from a few Hz to tens of KHz propagates in the form of impulsive signals which get reflected by the Earth (at the lower boundary) and the ionosphere (at the upper boundary) and thereby propagate in a guided fashion in the waveguide formed by the Earth and the ionosphere referred to as the Earth-Ionosphere waveguide. Due to their very low attenuation rate these sferics have the capacity to travel very long distances from their source lightning (in the order of thousands of kilometers) and thus can be observed very far away from their point of origin using appropriate VLF and ELF receivers.

The aim of this thesis is to model the ELF sferic waveforms up to a frequency of 500 Hz that could be observed at McMurdo Station in Antarctica, generated by rocket triggered lightning at the International Center for Lightning Research and Testing (ICLRT) at Camp Blanding, Florida. Rocket triggered lightning makes it possible to obtain accurate measurements of various parameters of lightning such as current and total charge transfer, which is not possible with natural lightning due to the unpredictable nature of its occurrence.

The modeling of the spheric waveform is carried on using the Long Wavelength Propagation Capability (LWPC) code developed by the Naval Ocean Systems Center over a period of many years. In order to do so, certain parameters are needed like the current waveform of the lightning and the ionospheric electron density profiles over the path of propagation. This work assumes that the lightning strike is a vertical dipole discharge and that the ionosphere is homogenous throughout the path of propagation. Realistic ionospheric electron density profiles were created using data from the International Reference Ionosphere (IRI), and realistic ground conductivity and permittivity profiles were considered that take into account different kinds of ground like land, sea, and ice.

The end result is the successful modeling of the time-domain magnetic field signature of a lightning strike triggered at the ICLRT after propagating more than 14 Mm to Arrival Heights at McMurdo Station, Antarctica. These theoretical results may be directly compared with future experimental observations.

## CHAPTER 1 INTRODUCTION

Lightning was at one point feared as an atmospheric flash of supernatural origins-the great weapon of the gods. It has been used to describe power and might in ancient mythologies. Greek mythology describes thunder and lightning as the mighty weapons of Zeus. In the Bible lightning is often depicted as a manifestation of the wrath of God. The vedas describe lightning as the weapon used by Indra, the king of heaven.

The scientific study of lightning has its modest beginning in the 18th century. Benjamin Franklin performed the first systematic study of lightning during the second half of 18th century. He was the first to design an experiment that conclusively proved the electrical nature of lightning. Little progress was made in understanding the properties of lightning until the late 19th century. Lightning current measurements were made in Germany by Pockels around 1900 who analyzed the magnetic field induced in materials by lightning to estimate the current values. There has been a rapid increase in the lightning related research in the past 30-40 years with the arrival of digital computers and of high speed data acquisition systems.

Lightning radiates electromagnetic energy over an extremely wide bandwidth from a few Hz ([Burke, 1992](#)) to many tens of MHz ([Weidman, 1986](#)). Most of the energy is radiated in the Very Low Frequency (3-30 KHz) and Extremely Low Frequency (3-3000 Hz) bands because of the sub-millisecond to millisecond time scales and several kilometer spatial extents of the radiating current ([Uman, 1987](#)). The energy radiated in the ELF/VLF bands is reflected by the ionosphere and the ground, thereby propagating in a guided fashion between the Earth and the ionosphere which form the Earth-ionosphere waveguide. The electromagnetic signals in the ELF/VLF bands generated by lightning are known as radio atmospherics or more commonly as sferics. These sferics propagate in the Earth-ionosphere waveguide with low attenuation rates around 2-3 dB per 1000 km and thus can be observed at great distances from their

origin (Davies, 1990). The characteristics of the sferic waveform are controlled by their source lightning discharges and the parameters of the Earth-ionosphere waveguide (Cummer, 1997).

This thesis focusses on modeling the ELF sferics generated due to rocket triggered lightning.

### 1.1 The Lightning Discharge

A thundercloud has a large positively charged layer and a negatively charged layer of about equal magnitude which forms an electric dipole (Rakov and Uman, 2003). Once these charged layers attain enough charge, the electric fields associated with the charges begin to exceed the dielectric breakdown voltage of the atmosphere, leading to the occurrence of a lightning flash.

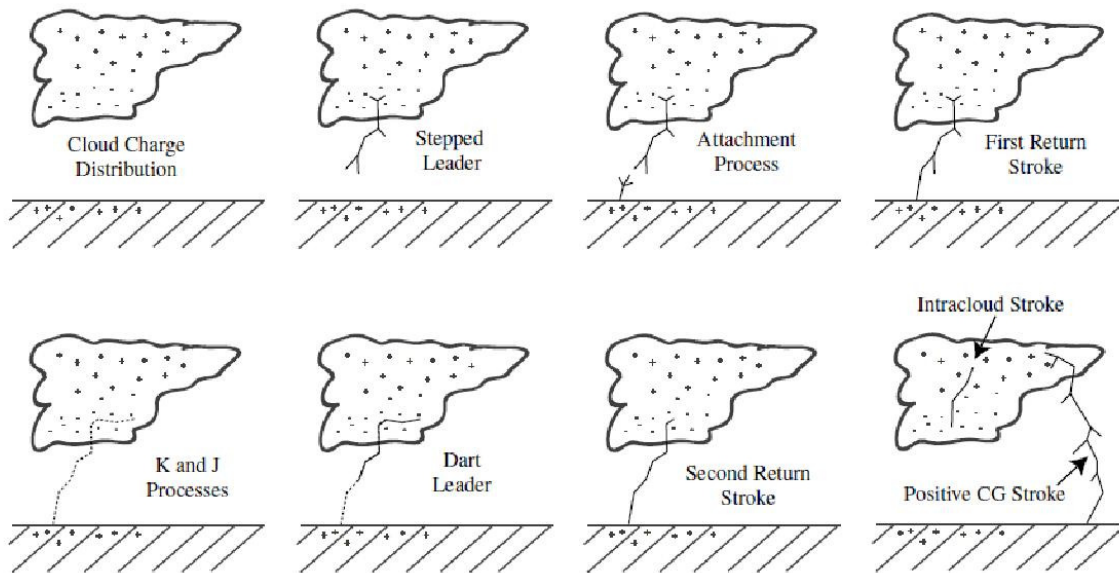


Figure 1-1. Various phases of a two stroke negative cloud to ground lightning discharge Adapted from Rakov and Uman-2003.

Lightning flashes are classified as:

- Cloud discharges: those that do not terminate on the surface of Earth, e.g., Intracloud discharges, Cloud to air discharges and intercloud discharges

- Cloud to Ground discharges: those with at least a partial discharge to ground, e.g., negative cloud to ground discharges, positive cloud to ground discharges

The cloud discharges are the most numerous type of lightning (50-75 percent) (Prentice and Mackerras, 1977). The cloud to ground discharges can be classified into two groups depending on the layer of charge they originate in. If the cloud to ground discharge originates in the negatively charged layer it is called negative cloud to ground flash, if the discharge originates in the positively charged layer it is called positive cloud to ground discharge (Wood, 2004). While 90 % of the cloud to ground flashes are negative discharges and the major portion of the remaining 10% are positive discharges. There are also discharges transporting both negative and positive charges to the ground, such discharges are very rare.

A negative cloud to ground discharge is illustrated in Figure 1-1. It is initiated when a stepped leader begins to work its way down from the cloud in a series of discrete steps after a preliminary breakdown in the negatively charged layer. As the stepped leader advances downward, the electric field between the end of the stepped leader and the ground becomes high enough that conductive leaders begin to reach upwards from the ground. When the stepped leader and the conductive leader close the 10-100 meters gap, attachment occurs, leading to the generation of the first return stroke of discharge. The return stroke involves the flow of large electric current from the ground to the cloud, thereby producing a radio atmospheric (Rakov and Uman, 2003). The first return stroke may deplete the layer of cloud charge thereby terminating the flash. If any additional charge is available, J and K processes occur which redistribute the remaining charge in the cloud. The conducting channel remains partially ionized following the first return stroke and a dart leader may reionize the channel resulting in a second stroke. This process repeats itself generating many return strokes (Uman, 1987). A similar process with usually one stroke occurs for positive cloud to ground discharges.

## 1.2 Rocket Triggered Lightning

It is necessary to observe lightning at close range to accurately investigate some of the associated phenomena, but natural lightning strikes at unpredictable times and places, making close observation by qualified people equipped at the time with necessary instrumentation unlikely. Rocket triggered lightning has been an important means to overcome that problem. Experiments years ago demonstrated that a lightning strike often can be triggered by launching a rocket connected to a long grounded copper wire toward a thunderstorm. A strike triggered that way tends to follow the wire. The wire quickly vaporizes and does not conduct a significant percentage of the lightning current. Its function is merely to guide a lightning strike to measuring equipment.

Rocket triggered lightning is produced in two methods currently ([Rakov and Uman, 2003](#)):

- Classical Rocket Triggered Lightning
- Altitude Rocket Triggered Lightning

### 1.2.1 Classical Rocket Triggered Lightning

In classical triggering method, the wire which is attached to the rocket is connected at the other end to a grounded launcher. An upward positive leader is generated at the tip of the rocket after it reaches an altitude of around 200 m. The current of the upward positive leader vaporizes the wire and an initial continuous current (ICC) follows for some hundreds of milliseconds. After the completion of the ICC phase, there exists a phase for a few tens of milliseconds where no current flows. This phase is followed by the generation of a leader-return stroke sequences. These are similar to the subsequent leader-return stroke sequences in natural lightning.

During the formation of the upward positive leader a phase called the Initial Current Variation (ICV) occurs when the triggering wire is replaced by the upward positive leader plasma channel. The upward positive leader produces current which is of the order of tens to hundreds of amperes (measured at ground) which vaporizes the wire. At this

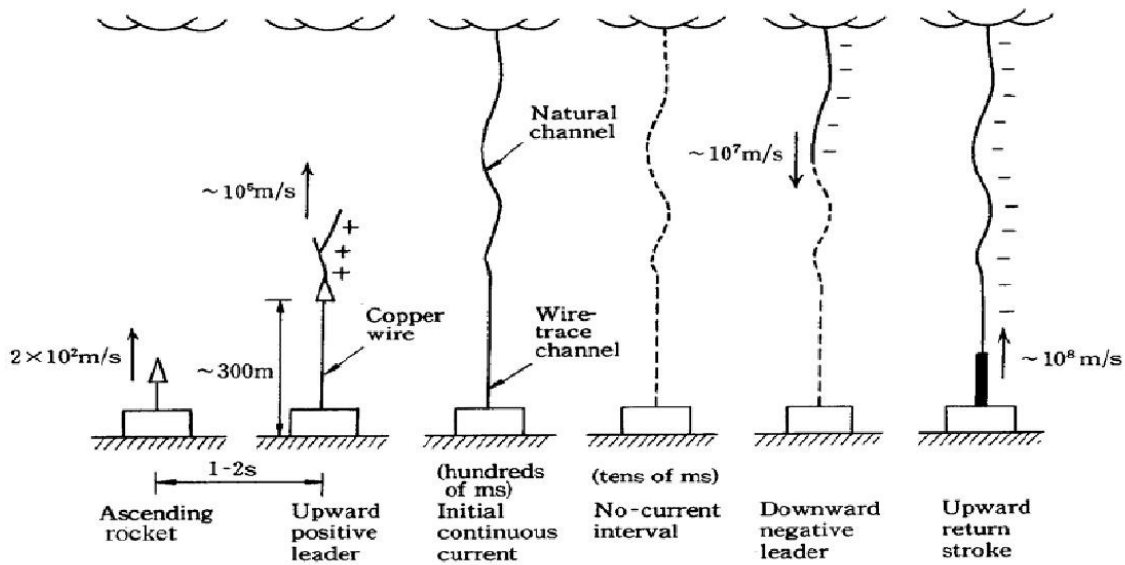


Figure 1-2. Classical Rocket Triggered Lightning (V.A.Rakov "Lightning Discharges Triggered Using Rocket and Wire Technique", J.Geophys.Res.,vol.100,pp.25711-25720,1999

instance the current measured at ground falls to zero approximately due to the absence of a conducting path. A downward leader process bridges the resultant gap and initiates a return stroke process from the ground which serves to re-establish the interrupted current flow to the ground.

### 1.2.2 Altitude Rocket Triggered Lightning

Altitude triggering technique uses an ungrounded wire. This enables the possibility to reproduce some features of first stroke of natural lightning which is not possible using classical triggering. The apparatus has a 50 m long copper wire connected to the ground launcher, a 400 m long insulating kevlar cable in the middle and 100-200 m long floating copper wire connected to the rocket. The upper floating wire is used for triggering while the lower grounded wire is used for intercepting the leader. When a rocket reaches a suitable altitude (around 600 m) a bi-directional leader composed of a upward positive leader and a downward negative leader is initiated. The electric

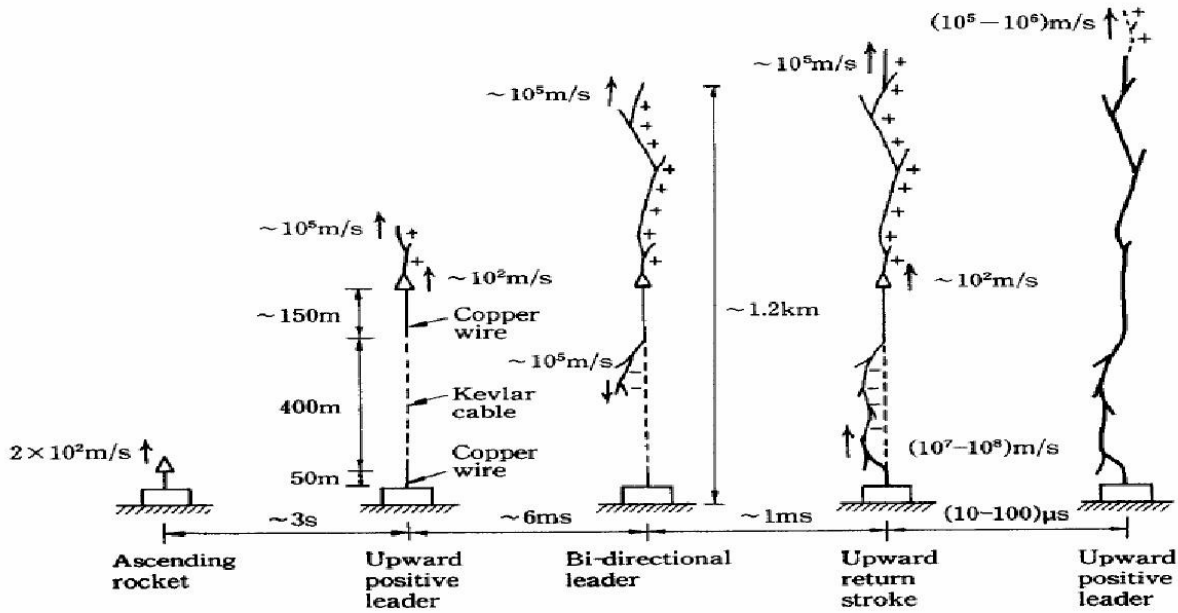


Figure 1-3. Altitude Rocket Triggered Lightning (V.A.Rakov "Lightning Discharges Triggered Using Rocket and Wire Technique", J.Geophys.Res.,vol.100,pp.25711-25720,1999

field produced by the downward negative leader initiates an upward connecting positive leader from the grounded copper wire. This connects to the downward negative leader and this process leads to the generation of a return stroke.

### 1.2.3 Current Waveforms

A typical negative rocket triggered lightning has been described to be similar to a upward initiated lightning from a tall structure (Uman, 1987). It involves an initial stage (IS) that is composed of an upward positive leader (UPL). It is followed by an initial continuous current (ICC). The ICC is commonly followed by a dart leader/return stroke sequences which are similar to the subsequent strokes in natural downward lightning. When there are no return strokes involved the triggered lightning event consists of the IS only and is termed as wireburn (D.Wang et al., 1999). It has been well documented in the literature that the ICC involves impulsive processes which are similar to the M-component pulses (Fieux et al., 1978).

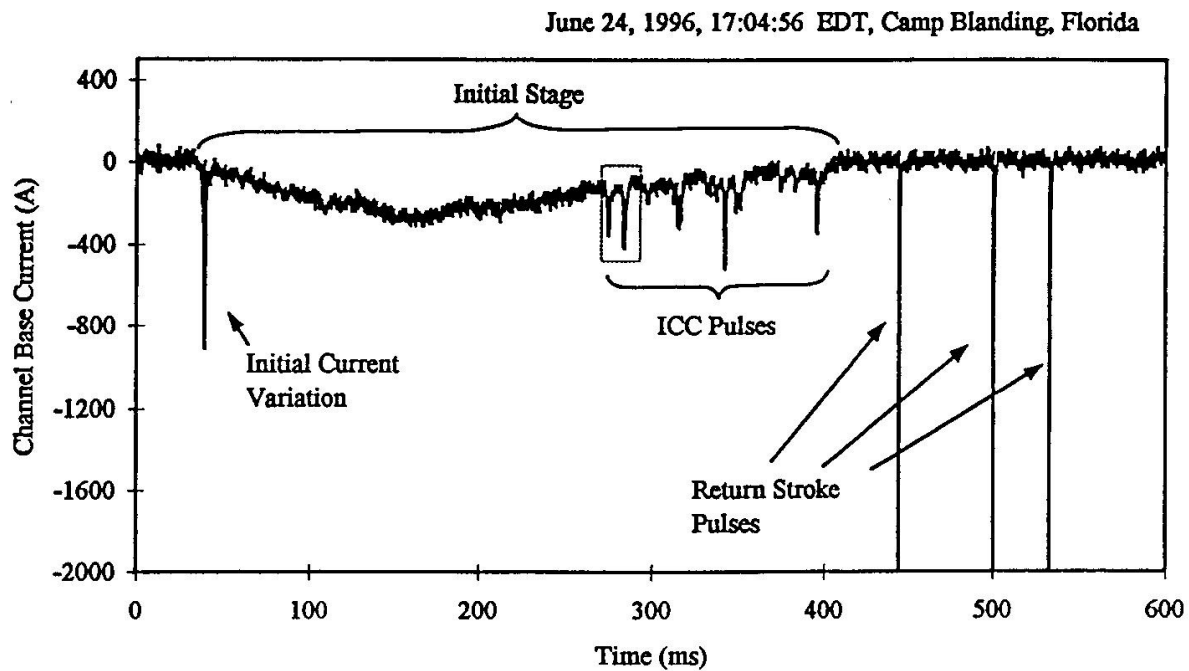


Figure 1-4. Overall current record of a triggered lightning at camp blanding, florida(D.Wang et al., "Characterization of initial stage of negative rocket triggered lightning", J.Geophys.Res.,vol.104,pg 4213-4222,1999)

Figure 1-4 indicates the various features associated with a typical negative rocket triggered lightning discharge. The initial stage in rocket triggered lightning is characterized by a channel base current having a duration of some hundreds of milliseconds and a magnitude of approximately 100 Amps. The pronounced current variation at the beginning of the IS is termed initial current variation (ICV), the ICV has a duration which typically does not exceed 10 ms (D.Wang et al., 1999). The ICV usually involves an abrupt decrease in current followed by a pulse. Alongside the ICV the IS typically includes a pronounced ICC.

### 1.3 Radio Atmospherics

Radio atmospherics or sferics in short are lightning produced electric and magnetic fields whose spectrum spans frequencies from a few Hz to a few hundreds of KHz. These are easily observed at distances spanning several thousand kilometers. Typical sferics have a frequency spectrum in the ELF (0-3 KHz) and the VLF (3-30 KHz) range,

but sometimes can extend into the LF (30-300 KHz) range ([Rakov and Uman, 2003](#)). Sferics propagate in the waveguide formed by Earth and ionosphere primarily by multiple reflections similar to a electromagnetic wave in a metallic waveguide. The early research in sferics began in the early 1900's and this primarily was a period of discovery. Strange noises were first observed on radio by German physicist Heinrich Barkhausen during world war I. A number of papers in the 1930's and early 1940's characterized and attempted to explain the received sferics from distant lightning sources. An important early paper on sferics ([Burton and Boardman, 1933](#)) describes two distinct emissions - "swishes" , "tweeks". The "swishes" are now referred to as "whistlers". During and in the period following World War II there was a great deal of interest in understanding the propagation of sferics, due to its implications regarding long-distance communication.

The study of ELF sferics, though fundamentally similar to the VLF sferics, mostly has been treated separately in the literature. ELF sferics are also referred to as slow tails and have been studied experimentally for many years [e.g., ([Hepburn, 1992](#)), ([Taylor and Sao, 1970](#)), ([Burke, 1992](#)) etc. ([Jones, 1974](#)) published a bibliography of experimental measurements of ELF propagation characteristics generated by lightning. ([Budden, 1961](#)) and ([Wait, 1970](#)) made a tremendous contribution in understanding the propagation of ELF and VLF sferics in the Earth-ionosphere waveguide.

Figure 1-5 shows a sferic waveform recorded at Palmer station Antarctica (adapted from .([Wood, 2004](#))). It clearly shows a VLF impulse followed by a ELF "slow tail" ([Reising et al., 1996](#)). The oscillatory nature of the VLF impulse is due to the presence of multiple modes of propagation, however the ELF component only has one mode of propagation (QTEM mode) ([Cummer, 1997](#)). The spectral content of sferics varies widely and there are many variations observed, a good analysis of some variations in sferics observed is described in ([Cummer, 1997](#)).

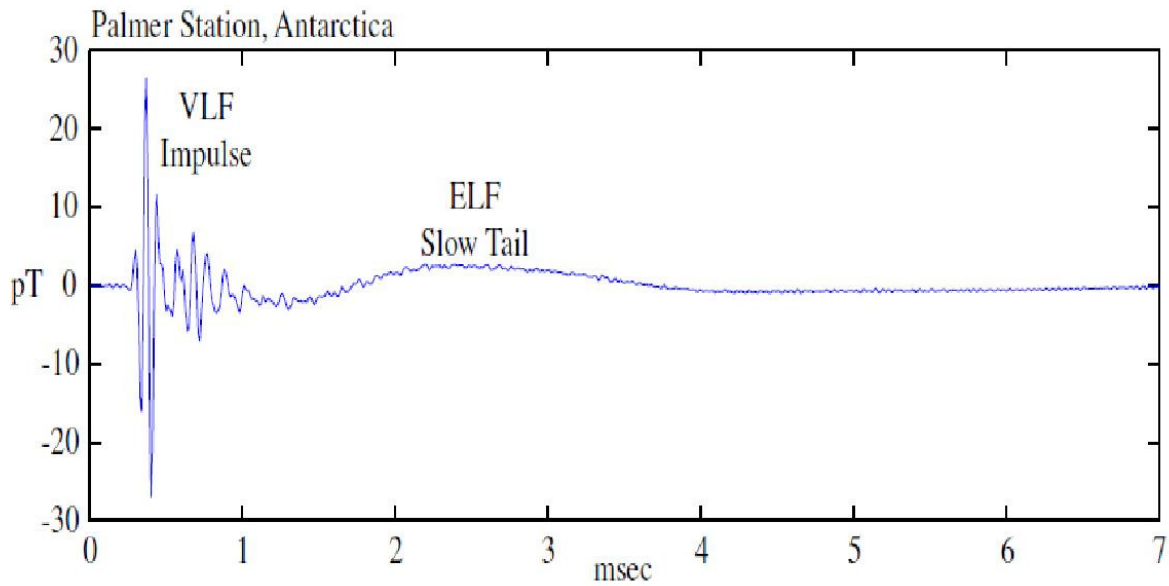


Figure 1-5. Time domain waveform of a sferic observed at palmer station (adapted from (Wood, 2004))

## 1.4 Ionosphere

The ionosphere is the uppermost part of the atmosphere stretching from a height of about 50 km to 1000 km that is ionized by the solar radiation. Even though the ionosphere forms only a small part of the atmosphere it has a very important role because of its influence on the radio waves (especially ELF and VLF waves). When solar radiation strikes the chemical constituents of the atmosphere, electrons are dislodged from atoms and molecules to produce the ionospheric plasma. The presence of these charged particles makes the ionosphere an electrical conductor which supports electric currents and generates radio waves.

Ultraviolet (UV), X-Ray, and shorter wavelength radiation from the sun have sufficient energy in them to dislodge an electron from a neutral atom or molecule and are mostly responsible for ionization. The amount of ionization primarily depends on the activity of the sun, it varies greatly with the amount of radiation received from the sun

and thus there is a diurnal effect, a seasonal effect and also varies with the geographic location (Davies, 1990).

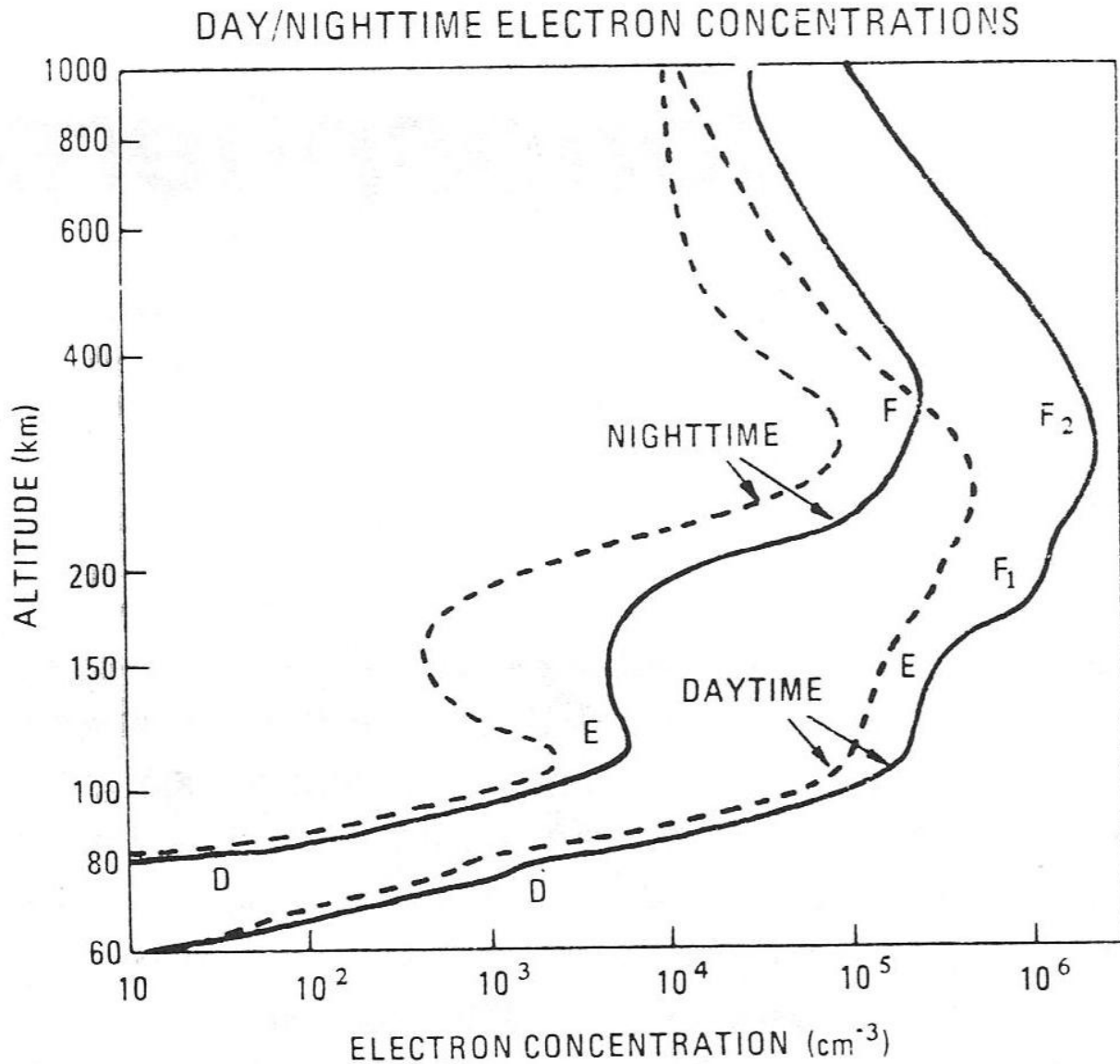


Figure 1-6. Day and Night time electron density profiles for sunspot maximum (solid lines) and sunspot minimum (dashed lines), adapted from Tascione, T.F., Introduction to the Space Environment, 2nd Ed.

The ionosphere is divided into regions (D-region, E-region and F-region) with a specific ionization. The lowest is the D-region covering the altitude 50 km-90 km, then comes the E-region between 90km-150km and finally the F-region (also known

as the Appleton layer) above the E-region. There are F1 and F2 regions within the F-region. The electron concentrations reach their highest levels in the F-region, more specifically the F2-region (Hargreaves, 1992). Figure 1-6 shows the electron density profiles of a typical ionosphere at both night time and day time at mid-latitude. The F1 layer disappears during the night while the F2 layer slowly decreases through the night.

The ionosphere is a dynamic medium and the study of the ionosphere is an important field. Ionospheric sounding is one of the oldest and most accurate ways of studying the ionosphere. In this technique ionosondes are employed in sending signals into the ionosphere which are reflected back in the presence of ionization, the frequency at which the reflection occurs gives information about the plasma density at the altitude. Ionosondes are effective in probing the E-region and the F-region but not the D-region (Hargreaves, 1992).

A more recent technique is the Incoherent Scatter Radar, the advantage with this technique being that it can probe the ionosphere beyond the F2 region electron density maximum and is capable of measuring other quantities such as electron temperatures etc (Evans, 1969). The disadvantage with this technique, however, is that it requires very expensive equipment and is not very useful in measuring the electron density levels at the lower levels. Measurements of the D-region are still very difficult and the techniques described above are not suitable for making measurements at D-region altitudes. Moreover the D-region is too low for rockets and too high for balloons to make any measurements. Thus one of the very few methods to study the D-region of the ionosphere is through VLF waves. The VLF waves are completely reflected by the ionosphere, and this makes them a very useful tool for measurements in D-region (Cummer, 1997). Long distance VLF propagation effects measured in sferics are an important source to make D-region measurements (Cummer, 1997). Recently a technique has been developed in which ELF wave propagation measurements made

using lightning discharges as a source are used in remote sensing the E-region of the ionosphere ([Cummer and Inan, 2000](#)).

CHAPTER 2  
INSTRUMENTATION AND LAYOUT AT MCMURDO STATION ANTARCTICA AND  
CAMP BLANDING

2.1 **McMurdo Station- Antarctica**

McMurdo Station is an American Antarctic research station located on the southern tip of Ross island on the shore of McMurdo Sound in Antarctica. It is operated by United States Antarctic Program, a branch of National Science Foundation and is the largest community in Antarctica which includes a harbor, 3 airfields, a heliport and over 100 buildings. The United States officially opened its first station in McMurdo on Feb 16, 1956 and it was initially called Naval Air Facility McMurdo.

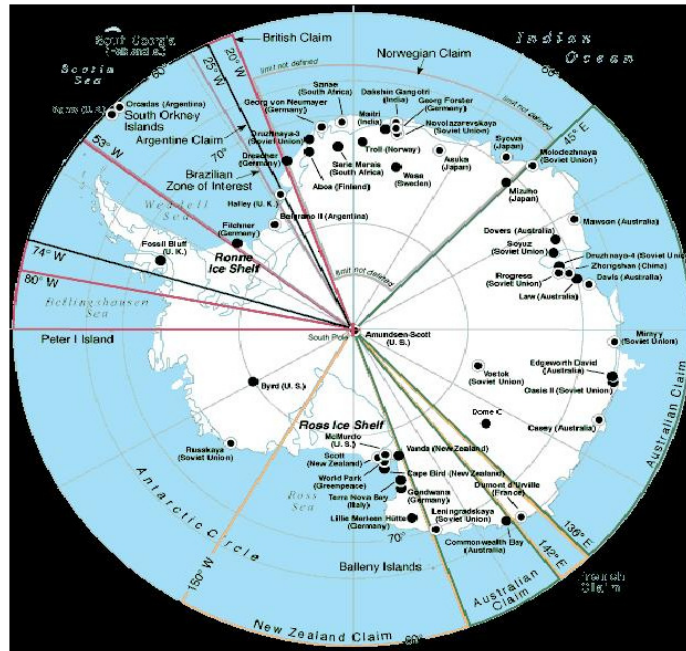


Figure 2-1. A map of Antarctica indicating Ross Island and McMurdo Station (source: <http://international.usgs.gov>)

Figure 2-1 indicates the location of Ross Island and McMurdo Station in Antarctica. Figure 2-2 shows a Landsat image of the Ross Island and this image points the location of McMurdo Station on Ross Island. Figure 2-3 shows a picture of the McMurdo Station taken from the observation hill. The buildings range in size from a small radio shack



Figure 2-2. A LandSat Map of Ross Island (source: <http://international.usgs.gov>)



Figure 2-3. A picture of McMurdo Station (source: <http://international.usgs.gov>)

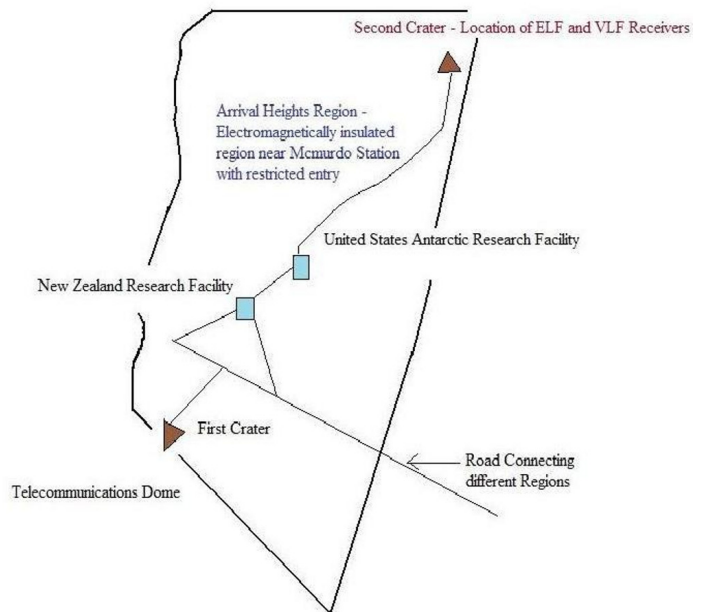
to large three storeyed structures. The buildings include repair facilities, dormitories, administrative buildings, a firehouse, power plant, water distillation plant, wharf, stores, clubs, warehouses and Crary Lab. These are linked by above ground water, sewer, telephone and power lines. The station covers an area of nearly 1.5 sq.miles.

### 2.1.1 Arrival Heights Area, McMurdo Station

McMurdo Station lies at an invariant magnetic latitude of about 80 degrees inside the polar cap at all local times and is a unique site for studying the natural phenomena and atmospheric studies, one of the main reasons for this is its location being remote from contamination sources. The projects that operate from the Arrival Heights area at McMurdo station examine natural phenomena that occur in the Earth's atmosphere and magnetosphere, Figure 2-4 shows a picture of this area and the map of this area. The map gives an idea of the various facilities at this area.



A Image of Arrival Heights Region, Photo by Seth White(Source:www.sethwhite.org)



B Map of Arrival Heights Region

Figure 2-4. Arrival Heights, McMurdo Station

The objectives of these programs include investigations of phenomena that couple solar processes into the terrestrial environment, which include processes with short term environmental effects such as the auroras and radio wave communication interference, as well as those associated with long term effects such as ozone layer and atmospheric composition studies. The instruments for these tasks include optical and radio devices for remote sensing, sensors for monitoring changes in electric and magnetic fields at the station, ELF-VLF receivers.

The signals from different instruments at the Antarctic observatories are recorded on a common data logger and can be shared. These instruments provide analog signals that are digitized and recorded by PC based systems recording to magnetic-optical disks. These data acquisition systems are operated at station facilities and record data from many instruments which include

- ELF-VLF receivers, University of Florida(Principle Investigator:Dr.Robert Moore)/Stanford University
- Riometers and Photometers, University of Maryland
- Searchcoil Magnetometer , University of New Hampshire
- Fluxgate Magnetometer , NJIT

### **2.1.2 ELF/VLF Research at McMurdo Station**

Historically, a major part of ELF/VLF research at Arrival Heights has been carried out by Stanford University (Antony Fraser-Smith). The University of Florida recently took control of these systems together with Stanford, providing much needed hardware upgrades to the systems. As a part of this program University of Florida set up receivers at Arrival Heights and South Pole station in January 2010, and at Palmer Station in May 2010.

The VLF receiver and ELF receiver at Arrival Heights are presently maintained and operated by Robert Moore of the University of Florida. Figure 2-5 shows image of the VLF receiver located in the second crater region (shown in the image of the map

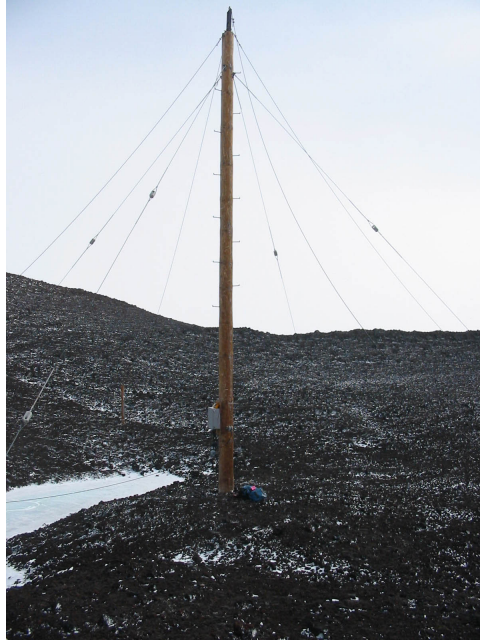


Figure 2-5. A picture of the VLF receiver at McMurdo Station, Photo by Seth White (Source:www.sethwhite.org)

of arrival heights in Figure 2-4 and Figure 2-6 shows the image of the ELF receiver at McMurdo Station.



Figure 2-6. A picture of the ELF receiver at McMurdo Station, Photo by Seth White (Source:www.sethwhite.org)

The ELF/VLF receiver systems at McMurdo Station record wave activity incident upon North/South and East/West crossed loop antennas shown in Figure 2-5 and Figure

2-6. A preamplifier is near the antenna and the remainder of the system is located in the hut shown in Figure 2-4. The racks shown in Figure 2-7 hold the line receiver, GPS timing unit, mixer/monitor and analog recorders.



Figure 2-7. A picture of the Racks that hold the data acquisition equipment at McMurdo Station, Photo by Robert Moore

The VLF receiver is located inside the second crater at Arrival Heights which is an old volcanic crater about 1.5 miles north of the hut shown in Figure 2-4. University of Florida and Stanford University are jointly running this project using the VLF and ELF antennas to measure the very long wavelength electromagnetic waves which propagate around the globe in the Earth-ionosphere waveguide. VLF receiver(Figure 2-5) consists of a central wooden pole mounted in the ground, and four triangular loops of wire run down to the ground from its top. The other four wires are support lines for the pole itself. The wire loops are oriented N-S and E-W and pick up radiation in the 3 KHz-30 KHz range.

Figure 2-6 shows the ELF receiver in the vault. Unlike the VLF antenna, which sways in the breeze, it is important for the ELF antenna to remain stationary and thus it was buried in a wooden vault out in the lava fields north of the hut. The antenna has two components, one oriented north-south and the other oriented east-west, and they pick up signals in the 1Hz - 3KHz range.

## 2.2 International Center for Lightning Research and Testing at Camp Blanding (ICLRT), Florida

A lightning research facility at Camp Blanding, Florida was started by Electric Power Research Institute (EPRI) and Power Technologies Inc in 1993. University of Florida and Camp Blanding Florida Army National Guard Base signed an agreement forming the International Center for Lightning Research and Testing (ICLRT) for the purpose of advancing the science and technology of lightning in October 1994. The center has an area of more than 100 acres, located about 45 km north-east of Gainesville (UF), Florida having the co-ordinates  $30^{\circ}$  N and  $82^{\circ}$  W. Since 2005 the facility is being jointly operated by University of Florida and Florida Institute of Technology. The site is ideal for conducting rocket triggered lightning experiments especially due to its restricted airspace (source of information, [www.lightning.ece.ufl.edu](http://www.lightning.ece.ufl.edu)). Figure 2-8 shows the overview and layout at Camp Blanding in 2002.

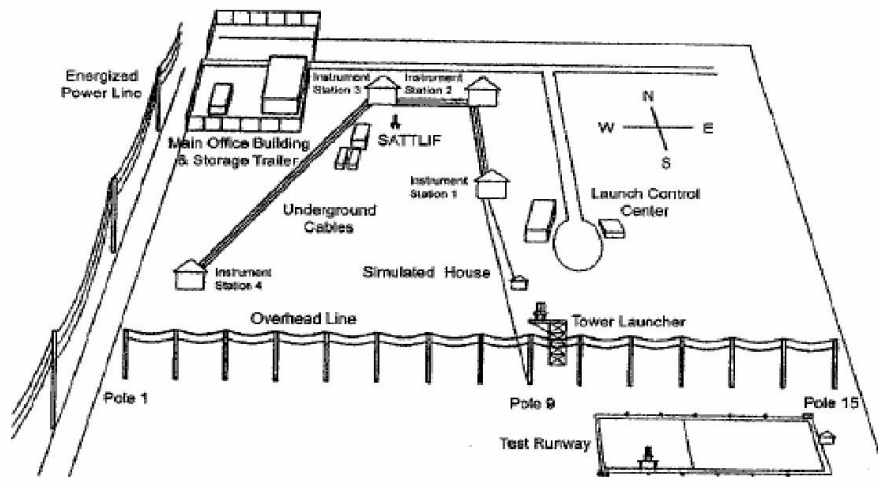


Figure 2-8. Overview of ICLRT at Camp Blanding in 2002, source:([Rakov et al., 2003](#))

infrastructure at ICLRT, Camp Blanding are:

- 2500 square-foot office building
- Two launch trailers
- One launch tower

- One mobile launcher
- four instrumentation buildings
- Two overhead test power lines
- A test airport runway
- An underground test power system

One of the primary goals of ICLRT is to study rocket triggered lightning and natural lightning. The current infrastructure at ICLRT has 91 measurements, digitization and control computers which enable the study of both triggered and closely occurring natural lightning, eg ([Rakov and Uman, 2003](#)) and ([Crawford et al., 2001](#)). These instruments measure electric and magnetic fields, high energy radiations (X-rays), optical radiation and channel-base currents.

At ICLRT different types of digital storage oscilloscopes (DSO) are employed to digitize and store data. The DSOs are armed, calibrated and disarmed by a central computer in launch control (HAL) via GPIB or ethernet, once armed the DSOs are triggered to record data when the channel based currents exceed 6 kA or when the two optical sensors placed in the corners of the site and pointing towards the launch tower detect luminosity exceeding a certain threshold value simultaneously. Both these conditions indicate the occurrence of either triggered or natural lightning.

A separate network of DSOs called Positive Lightning Experiment (POE) is setup to record data from off-site positive cloud-to-ground lightning without preventing the acquisition of data from on-site lightning

Details of the DSOs used at ICLRT:

- 2 Yokogawa DL716 16 channel instruments with 10 MHz sampling rate and 4 MHz bandwidth
- 5 Yokogawa DL750 16 channel instruments with 10 MHz sampling rate and 3 MHz bandwidth

- 4 LeCroy LT344L 4 channel instruments with 250 MHz sampling rate and 20 MHz bandwidth
- 2 LeCroy LT374L 4 channel instruments with 250 MHz sampling rate and 20 MHz bandwidth
- 4 LeCroy 44Xi 4 channel instruments with 250 MHz sampling rate and 20 MHz bandwidth

Two different types of devices are used to measure channel base currents. These currents are measured at the bottom of the launch tubes located atop the launch tower. The first current measuring device is a low inductance current viewing resistor model R-7000-10. The second device is a clamp-on current transformer, a model 6801 custom manufactured by Pearson Electronics.

ICLRT has three field mills (a device used to sense static fields) deployed at the site with the purpose of determining the availability of suitable thunderstorm conditions for triggering lightning (electric field values between 4-10 kV/m). Ground-level and broadband vertical electric field and field derivatives are sensed using flat-plate sensors. Currently there are eight dE/dt sensors and ten electric field sensors at the site.

Two high speed video cameras with adjustable framing rates and pixel resolution are used to image the lower several hundred meters of lightning channel. One of the cameras used is a Photron SA1.1 and the other is Phantom v7.3, the Photron operates at a faster framing rate than the Phantom, it is used to record videos at speeds up to 300,000 frames-per-second (fps) of the lowest hundred meters of the triggered lightning channel with a horizontal field-of-view of tens of meters. The Phantom is generally operated at speeds up to 10 kfps of the bottom several hundred meters of the channel with a horizontal field-of-view of about hundred meters (courtesy Chris Biagi, Lightning Lab, University of Florida).

Figure 2-9 shows a satellite image of ICLRT at Camp Blanding, Florida and indicated in it are some of the major structural landmarks, this figure is adapted from (Howard, 2009) and is taken from Microsoft Virtual Earth.



Figure 2-9. Satellite image of ICLRT with some of its major landmarks indicated, adapted from (Howard, 2009)

There are three ways to trigger lightning at ICLRT: (i) Underground Launcher (ii) The launch Tower (shown in Figure 2-10) (iii) A mobile launcher. Since 2005 only the launch tower and the mobile launcher have been used, the majority of the triggering being conducted at the tower (Howard, 2009). All the launchers are equipped with resistive shunts to measure the lightning channel base currents. The launch tower is a 11m tall wooden tower with the launcher on its top and and the tower is located near the launch control trailer as shown in Figure 2-8.

The launch control trailer shown in Figure 2-11 is the center of the triggering operations, it is located approximately 50 m north of launch tower. This building contains the launcher controls and also provides the electromagnetic shielding for the video and data acquisition equipment (Howard, 2009). The trailer is powered by a diesel generator during the triggering operations so that the equipment inside is not affected by a surge or failure in the power grid, both of which occur commonly during lightning (Howard, 2009).



Figure 2-10. A picture of launch tower, Source:Lightning Lab-University of Florida



Figure 2-11. Picture of launch control trailer, Source:Lightning Lab-University of Florida

A network of sensors used to collect electric and magnetic fields, time derivatives of the fields and X-ray emissions is in use at ICLRT and is known as the MSE(Multiple Station Experiment)/TERA(Thunderstorm Energetic Radiation Array). The MSE network (primarily composed of the electric and magnetic field and its time derivatives sensors) is maintained and operated by the University of Florida while the TERA network (primarily consisting of X-ray sensors) is operated by Florida Institute of Technology (Dwyer et al., 2004). A video system was also deployed as a part of this system which consisted of four camera sites whose signals were also triggered. The data from the network is also provided a GPS time stamp, allowing the data to be correlated with other systems such as the National Lightning Detection Network (NLDN) (J.Jerauld et al., 2005).

This whole system is operated through a control system which provides remote capability for many tasks like powering measurements, measuring battery voltages, monitor local thunderstorm conditions by measuring the quasi-static electric field at ground and automatically arm and disarm the network when appropriate (Howard, 2009). The electric and magnetic field, optical, and TERA measurements were sampled continuously for 2 s with 1s pre-trigger at 10 MHz on Yokogawa DL750 digital oscilloscopes, the  $dE/dt$  and TERA measurements are sampled by LeCroy digital oscilloscopes at 250 MHz. The channel-base current of the rocket-triggered lightning was recorded on both LeCroy and Yokogawa oscilloscopes. For a detailed report on the instrumentation at ICLRT the reader is recommended to refer (Howard, 2009).

## CHAPTER 3 ELF PROPAGATION IN THE EARTH-IONOSPHERE WAVEGUIDE

Extremely Low Frequency (ELF) electromagnetic waves lie in the frequency range 3 Hz to 3 KHz and are of interest in the fields of long distance communications and submarine communications due to their capability to propagate very long distances because of low attenuation rates and their capability to penetrate well through conducting materials. The most common and powerful source of electromagnetic radiation in the ELF and VLF range of frequencies is lightning.

ELF energy radiated from a lightning strike propagates in a guided fashion in the Earth-Ionosphere waveguide reflecting multiple times between the Earth and the ionosphere. ELF wave propagation in the Earth-Ionosphere waveguide depends on the electrical properties of the Earth and the ionosphere (here the boundaries of the waveguide) and the variable nature of the ionosphere. The attenuation rate of the wave is highly variable and is dependent on many factors like frequency, conductivity of the Earth, conductivity profile of ionosphere, reflection height of the ionosphere, and Earth's magnetic field. All these factors have a significant effect on the spheric waveforms observed from a distant lightning strike.

This chapter discusses the modal content in the ELF range of frequencies and gives a mathematical description of ELF wave propagation in the Earth-ionosphere waveguide. The waveguide mode theory (Budden, 1961) provides an analytical description of propagation of ELF/VLF waves.

### **3.1 Wave Propagation in an Ideal Parallel Plate Waveguide**

Consider an ideal parallel plate waveguide with its boundaries at  $x=0$  and  $x=a$  as shown in Figure 3-1 and assume the medium is lossless, simple and source free. The solution is obtained in a rectangular co-ordinate system, even though the Earth-Ionosphere waveguide is not flat (especially at very large distances considered here). A direct solution in the Cartesian co-ordinate system would be extremely

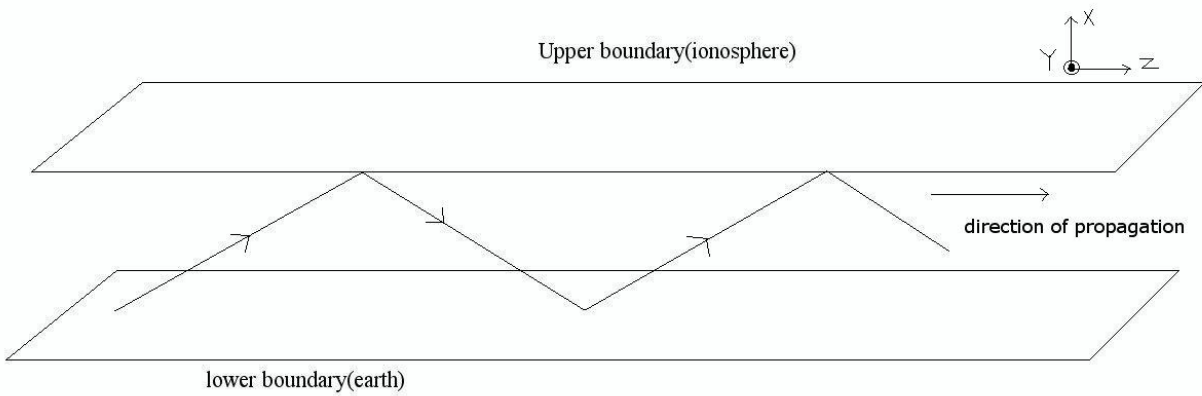


Figure 3-1. Ideal Parallel Plate Waveguide

complicated for the geometry. The waveguide is initially assumed to be perfectly flat and appropriate corrections are made later in the derivation for a spherical geometry (Budden, 1961).

The boundary conditions that are to be satisfied are  $E_{\text{tangential}}=0$  and  $H_{\text{normal}}=0$ .

The solutions for this problem can be divided into 3 categories:

- Transverse Electric (TE) Modes, in this case  $E_z=0$  and  $H_z \neq 0$
- Transverse Magnetic (TM) Modes, in this case  $H_z=0$  and  $E_z \neq 0$
- Transverse Electric and Magnetic (TEM) Modes, in this case  $E_z=0$  and  $H_z = 0$

Where modes are specific cases for which such waves can exist and there exists a condition which must be satisfied for a mode to exist which is the mode equation given below for each category.

Solution for  $TE_m$  modes

$$E_y = K_1 \sin\left(\frac{m\pi x}{a}\right) e^{-\gamma z} \quad (3-1)$$

The solutions for  $H_z$  and  $H_x$  can be obtained from equation 3-1 and Maxwell's equations. The mode condition for  $TE_m$  modes is given by

$$\sin(ah) = 0 \text{ or } ah = m\pi \text{ where } m = 0, \pm 1, \pm 2 \text{ etc} \quad (3-2)$$

Solution for  $TM_m$  modes

$$H_y = K_2 \cos\left(\frac{m\pi x}{a}\right) e^{-\gamma z} \quad (3-3)$$

The solutions for  $E_z$  and  $E_x$  can be obtained from equation 3-3 and Maxwell's equations. The mode condition for  $TM_m$  modes is given by

$$\sin(ah) = 0 \text{ or } ah = m\pi \text{ where } m = 0, \pm 1, \pm 2 \text{ etc} \quad (3-4)$$

Solution for TEM mode

It is a subset of  $TM_m$  mode solution, i.e.,  $TM_0$

$$H_y = K_3 e^{-\gamma z} \quad (3-5)$$

$$E_x = \frac{\gamma}{j\omega\epsilon} K_3 e^{-\gamma z} \quad (3-6)$$

Here  $\gamma$  is the propagation constant. The TEM mode is a special case of a TM mode. Both the electric and magnetic fields are transverse (perpendicular) to the direction of propagation for the TEM mode.

Waveguide modes can be numbered by the values of  $\theta$  (here  $\theta=ah$  in the example), the lowest value of  $\theta$  that satisfies the mode condition being the lowest order mode. Also different frequencies have different values of  $\theta$  associated with them. At certain frequencies the value of  $\theta$  reach  $90^\circ$  thereby preventing the waves from propagating, such frequencies are known as cut-off frequencies. When the frequency of the wave is below the cut-off frequency only complex values of  $\theta$  are possible and only

evanescent waves can exist in the waveguide. In an ideal parallel plate waveguide the TEM mode does not have a cut-off frequency and  $\theta=0$  for all frequencies.

The group velocity of a waveguide mode is:

$$v_g = c \cos \theta = c \sqrt{1 - \left(\frac{f_{cn}}{f}\right)^2} \quad (3-7)$$

Here  $f_c$  is the cut-off frequency for the  $n^{\text{th}}$  order mode. It can be observed from equation 3-7 that as frequency ( $f$ ) becomes approaches the cut-off frequency( $f_c$ ) the group velocity( $v_g$ ) approaches zero and as the value of  $f$  becomes much greater than  $f_c$ ,  $v_g$  approaches the speed of light. The TEM mode propagates at the speed of light with all the frequencies arriving simultaneously. The Earth-Ionosphere waveguide is far from an ideal waveguide, but the modal features exhibited by the ideal waveguide are similar to the modal features of the Earth-Ionosphere waveguide.

### 3.2 Wave Propagation in Plasma

The ionosphere that makes up the upper boundary of the Earth-Ionosphere waveguide is made up of cold plasma, hence it is necessary to understand the electromagnetic properties of cold plasma to understand the propagation of electromagnetic waves in the Earth-Ionosphere waveguide. Plasmas are the fourth state of matter and are considered to be special cases of gases that include a large number of electrons, ionized atoms, neutral atoms and molecules. In a more general sense a plasma is a state of matter that contains enough number of charged particles so that its dynamic behavior would be dominated by electromagnetic forces.

The sun and the stars are hot enough to be almost completely ionized with enormous densities and the interstellar gas is sparse enough to be almost completely ionized by stellar radiation. Starting from an altitude of 60 km the sun effects our atmosphere with a variety of radiations and the UV radiation is absorbed by the gaseous mixture in the atmosphere. In this process a large number of molecules and atoms receive sufficient energy to be ionized with maximum ionization occurring at an altitude

of approximately 350 km and this results in the formation of the ionosphere (Inan and A.S.Inan., 1999).

To determine propagation of electromagnetic waves in plasma Maxwell's equations along with equations of motion are required. The motion of electrons under the influence of electric and magnetic fields constitute which must be accounted for in Maxwell's equations through the current density term  $\bar{J}$ , which is given by:

$$\bar{J} = N_e q_e \bar{v} \quad (3-8)$$

Where  $N_e$  is the ambient electron density,  $\bar{v}$  is the velocity of electrons and  $q_e$  is the charge on a single electron. Similar relations can be deduced for motion of ions, but the current density due to ions is small and negligible compared to that of electrons.

The time harmonic form of Maxwell's equations can now be written as (Inan and A.S.Inan., 1999):

$$\nabla \times \mathbf{H} = j\omega\epsilon_0 \mathbf{E} + N_e q_e \mathbf{v} \quad (3-9)$$

$$\nabla \times \mathbf{E} = j\omega\mu_0 \mathbf{H} \quad (3-10)$$

$$\nabla \cdot \mathbf{E} \approx \frac{n_e q_e}{\epsilon_0} \quad (3-11)$$

$$\nabla \cdot \mathbf{H} = 0 \quad (3-12)$$

$$q_e \mathbf{E} \approx j\omega m_e \mathbf{v} \quad (3-13)$$

the continuity equation for electrons would be:

$$\nabla \cdot (N_e \mathbf{v}) = -j\omega n_e \quad (3-14)$$

From the Maxwell's equations above, the following equation can be deduced:

$$\nabla \times \mathbf{H} = j\omega\epsilon_0 \left(1 - \frac{N_e q_e^2}{\omega^2 m_e \epsilon_0}\right) \mathbf{E} \quad (3-15)$$

The above equation clearly indicates plasma can be represented by an effective dielectric permittivity given by (Inan and A.S.Inan., 1999):

$$\epsilon_{eff} = \epsilon_0 \left(1 - \frac{\omega_p^2}{\omega^2}\right) \quad (3-16)$$

where  $\omega_p = \sqrt{\frac{N_e q_e^2}{m_e \epsilon_0}}$  is called the plasma frequency. Thus the effects of plasma on the electromagnetic wave propagation can be represented in terms of the effective dielectric permittivity ( $\epsilon_{eff}$ ) and the solutions for fields can be obtained in a manner similar to that of air after replacing  $\epsilon_0$  with  $\epsilon_{eff}$ .

### 3.2.1 Effect of Collisions

Some electromagnetic power is always lost (i.e, transformed into heat) in a plasma because of the effects of collisions between electrons and molecules, ions and other electrons (Inan and A.S.Inan., 1999). The effect of these collisions are accounted for in the equation of motion through a frictional term, shown below.

$$q_e \mathbf{E} = j\omega m_e \mathbf{v} + m_e \nu \mathbf{v} = j\omega m_e \left(1 - j\frac{\nu}{\omega}\right) \mathbf{v} \quad (3-17)$$

where  $\nu$  is the collision frequency. Solving the equations we can account for the effect of these collisions in the plasma in the effective dielectric constant in a manner similar to the one described previously, the effective dielectric constant ( $\epsilon_{eff}$ ) is given by:

$$\epsilon_{eff} = \epsilon_0 \left(1 - \frac{\mathbf{X}}{1 - j\mathbf{Z}}\right) = \epsilon'_{eff} - j\epsilon''_{eff} \quad (3-18)$$

where  $\mathbf{X} = \frac{\omega_p^2}{\omega^2}$  and  $\mathbf{Z} = \frac{\nu}{\omega}$ . In the above equation the imaginary part  $\epsilon''_{eff}$  represents the power loss due to collisions resulting in the attenuation of the wave. The expressions for an electromagnetic wave in a plasma with collisions can be deduced similar to that of a lossy medium using the above values (Inan and A.S.Inan., 1999).

### 3.2.2 Effect of Static Magnetic Field

When a steady magnetic field permeates a plasma (like in the case of Earth's magnetic field permeating the ionosphere), the medium becomes anisotropic and this

results in the permittivity being represented as a tensor (a matrix) and not a vector anymore (Inan and A.S.Inan., 1999). The effective permittivity ( $\epsilon_{eff}^{\equiv}$ ) can be represented as shown below:

$$\epsilon_{eff}^{\equiv} = \begin{pmatrix} \epsilon^{11} & \epsilon^{12} & 0 \\ \epsilon^{21} & \epsilon^{22} & 0 \\ 0 & 0 & \epsilon^{33} \end{pmatrix} \quad (3-19)$$

Where

$$\epsilon^{11} = \epsilon^{11} = \epsilon_0 \left( 1 + \frac{\omega_p^2 (1 - j\mathbf{Z})}{\omega_c^2 - (1 - j\mathbf{Z})\omega^2} \right) \quad (3-20)$$

$$\epsilon^{12} = -\epsilon^{21} = \epsilon_0 \left( \frac{j\omega\omega_p^2 \left( \frac{\omega_c}{\omega} \right)}{\omega_c^2 - (1 - j\mathbf{Z})\omega^2} \right) \quad (3-21)$$

$$\epsilon^{33} = \epsilon_0 \left( 1 - \frac{\omega_p^2}{\omega^2 (1 - j\mathbf{Z})} \right) \quad (3-22)$$

Using the above terms and solving for the fields the value of index of refraction ( $n$ ) can be derived and is given below.

$$n^2 = 1 - \frac{\mathbf{X}}{\mathbf{U} - \frac{Y^2 \sin^2 \theta}{2(U-X)} \pm \sqrt{\frac{Y^4 \sin^4 \theta}{4(U-X)^2} + Y^2 \cos^2 \theta}} \quad (3-23)$$

where  $\mathbf{X} = \frac{\omega_p^2}{\omega^2}$ ,  $\mathbf{Y} = \frac{\omega_c}{\omega}$ ,  $\mathbf{Z} = \frac{\nu}{\omega}$ ,  $\mathbf{U} = 1 - j\mathbf{Z}$  and  $\theta$  is the angle between direction of propagation and the static magnetic field.

The above equation is known as the Appleton-Hartree equation. It could be observed that it has two roots corresponding to two characteristic waves.

### 3.3 Properties of Earth-Ionosphere Waveguide

The Earth-Ionosphere waveguide is significantly different from the ideal parallel plate waveguide because of the electrical properties of the Earth, ionosphere and the presence of Earth's magnetic field. In the Earth-Ionosphere waveguide, the boundaries i.e., the Earth and the ionosphere are not perfect conductors. The Earth has a finite conductivity which varies greatly depending on whether the particular location is land,

sea or ice and also on the type of soil and on many other factors. The conductivity of Earth is relatively low when compared with that of a good metallic conductor, but at ELF frequencies Earth behaves as a good conductor. But the waves propagating in the Earth-Ionosphere have some amount of attenuation.

The ionosphere which is the upper boundary of the Earth-ionosphere waveguide is an ionized region of the upper atmosphere that contains significant number of free electrons and ions (Hargreaves, 1992). This makes the region behave like a plasma, the presence of the Earth's magnetic field makes the ionosphere an anisotropic medium (whose properties are discussed in the previous section).

There are two important works dealing with the propagation of ELF and VLF waves in the Earth-ionosphere waveguide. The work of James Wait published in many scientific papers during 1960's and 1970's and summarized in his book (Wait, 1970). Wait deals with the presence of ionosphere (upper boundary of the waveguide) as not a single layer but rather as a series of interfaces and thereby correctly approximating a smoothly varying ionosphere, but he fails in correctly interpreting the effect of the presence of Earth's magnetic field in the ionosphere by describing the medium as an isotropic medium whereas in reality it is an anisotropic medium. The other prolific publisher in this field is K.G.Budden who developed a theory which is summarized in his book (Budden, 1961) called "waveguide mode theory of wave propagation" to correctly describe the propagation of ELF/VLF waves in the Earth-Ionosphere waveguide.

### **3.4 Waveguide Mode Theory-Budden.K.G**

#### **3.4.1 Sources of Waves- The Hertzian Dipole**

The spheric signal is highly dependent on certain parameters of source lightning (especially the time derivative of current  $\frac{\partial I}{\partial t}$  and current I) through which it originates. The simplest kind of source in electromagnetism is Hertzian dipole which is equivalent to having two equal and opposite charges  $\pm q$  on conductors placed very close together and joined by a wire (Budden, 1961). A vertical dipole is one whose axis is parallel to

the line which is vertically upwards from the lower boundary (here Earth) and pointing towards the upper boundary (here ionosphere), perpendicular to the surface of the boundary (assuming the surface is flat). A radio transmitter is often modeled as a vertical dipole and is applicable especially when the dimensions of the transmitting aerial are small compared to the wavelength, hence this idea is applicable especially at extremely low frequencies and very low frequencies (Budden, 1961). The waveguide mode theory is applicable at ELF/VLF frequencies and hence when dealing with this spectrum of frequencies the source can safely be approximated as a vertical Hertzian dipole.

At very low frequencies a transmitting aerial is generally a bundle of wires connected to a transmitter with its other terminal connected to Earth. Taking Earth to be a perfect conductor the charge on the wires induces an equal and opposite image charge in the Earth's surface thereby forming a dipole which to a certain degree is equivalent to a Hertzian dipole (Budden, 1961). The aerial itself was a half-dipole its image in the Earth's surface forming the other half. Budden states that a thunder cloud discharging to Earth is also similar to the half dipole aerial.

Since the expressions for electric and magnetic fields radiated by a Hertzian dipole are rather complicated, it is recommended by Budden to use another vector called the Hertz vector represented by  $\mathbf{U}$ . The electric and magnetic fields radiated by a Hertzian dipole are derived from the following expressions (Budden, 1961).

$$\mathbf{E} = -\mu \frac{\partial^2 \mathbf{U}}{\partial t^2} + \frac{1}{\epsilon} \nabla(\nabla \cdot \mathbf{U}) \quad (3-24)$$

$$\mathbf{H} = (\sqrt{\mu\epsilon}) \frac{\partial}{\partial t} \nabla \times \mathbf{U} \quad (3-25)$$

### 3.4.2 Modes in the Waveguide

If a half-dipole is placed near the Earth's surface (like a thundercloud) and it was said in the previous section that it radiates in a manner very similar to the Hertzian dipole. This section deals with relative amplitudes and excitation factors of the various

waveguide modes excited by the source assuming that the ionosphere is a perfect conductor at a certain height as well as the surface of the Earth as discussed by Budden in (Budden, 1961). The relative strength of the waveguide mode at a certain distance from the source is dependent on the orientation of the source and also on the angle of propagation.

Budden uses the fact that fields created by a source (here a half-dipole) between two conductors and the reflections due to these conductors is equivalent to the fields due to the source and its images. For example if there are two conductors at  $z=0$  and  $z=h$  and a source is present at  $z=0$ , it is equivalent to having a source at  $z=0$  and image sources at  $z=\pm 2h, \pm 4h, \dots$  with the conductors removed. This arrangement of the source and its images is similar to the effect of an optical diffraction grating (Budden, 1961).

Budden observed after solving for the Hertz vector in the above described scenario that in an ideal parallel plate waveguide vertical sources excite only TEM and  $TM_n$  waveguide modes whose relative amplitudes are given by :

$$\frac{1}{2} \rightarrow TEM \text{ mode} \quad (3-26)$$

$$(\cos \theta_n)^{\frac{1}{2}} \cos(kz_1 \sin \theta_n) \rightarrow TM_n \text{ mode} \quad (3-27)$$

where  $z_1$  is the height of the source with the lower boundary of the waveguide (the surface of Earth) being at  $z=0$ . It could also be observed from equation 3-26 that the TEM mode irrespective of the frequency of propagation has a gain of 1/2. The factor  $\cos(kz_1 \sin \theta_n)$  is also called as the excitation factor or the height gain function for the  $TM_n$  mode.

In a similar manner it was observed by Budden that horizontal sources excite only TE waveguide modes in an ideal waveguide with perfectly conducting parallel plate waveguide, whose relative amplitudes are given below :

$$(\cos \theta_n)^{\frac{-1}{2}} \sin(kz_1 \sin \theta_n) \rightarrow TE_n \text{ mode} \quad (3-28)$$

In equation 3-28  $\sin(kz_1 \sin \theta_n)$  is the height gain function for  $TE_n$  mode.

### 3.4.3 Reflection Coefficients in the Earth-Ionosphere waveguide

The upper boundary of the Earth-Ionosphere waveguide i.e., the ionosphere behaves like an anisotropic medium in the presence of the Earth's magnetic field which results in the fact the TE and TM modes are coupled at this boundary and an incident TE wave (or a TM wave) produces both TE and TM wave (Budden, 1961). Another way of looking at this is when an incident wave is polarized with a parallel polarization (or a perpendicular polarization) the wave reflected from the upper boundary is elliptically polarized with components that have both parallel and perpendicular polarizations. This effect can be accommodated for in the reflection coefficients. For the upper boundary (the ionosphere) the coupling between the modes results in the reflection coefficient ( $\mathbf{R}_U(\theta)$ ) no longer remaining a scalar but represented by a  $2 \times 2$  matrix and the reflection coefficient lower boundary (the Earth -  $\mathbf{R}_L(\theta)$ ) is not an anisotropic medium resulting in no coupling between the modes and the off-diagonal elements turning zero (Budden, 1961) with each element in the reflection matrices being a function of the angle of incidence to the respective boundaries.

The reflection coefficients for both the upper and lower boundaries ( $\mathbf{R}_U(\theta)$  and  $\mathbf{R}_L(\theta)$ ) as given by Budden are given below:

$$\mathbf{R}_U(\theta) = \begin{pmatrix} \parallel \mathbf{R}_{\parallel} & \parallel \mathbf{R}_{\perp} \\ \parallel \mathbf{R}_{\perp} & \perp \mathbf{R}_{\perp} \end{pmatrix} \quad \mathbf{R}_L(\theta) = \begin{pmatrix} \parallel \mathbf{R}_{\parallel}(\theta) & 0 \\ 0 & \perp \mathbf{R}_{\perp} \end{pmatrix} \quad (3-29)$$

In the above matrices the left subscript on the elements denotes the incident wave polarization and the right subscript denotes polarization of the reflected wave.

Due to the anisotropic nature of the ionosphere pure TE and TM modes are not capable of existing in the waveguide and instead the waveguide is composed of the modes called quasi-TEM (QTEM), quasi-TE (QTE) and quasi-TM (QTM) modes. The difference between a TE mode and a TEM mode for example is that the QTE mode is similar to a TE mode except that QTE mode also has a small axial electric field component (Budden, 1961). The lower order quasi modes are generally more pure than the higher order modes.

#### 3.4.4 Mode Equation

As stated in the previous section on parallel plate waveguides, for a mode to exist in a waveguide it has to satisfy the mode equation (like 3-2). But the boundaries of the Earth-Ionosphere waveguide are non-ideal and are much more complicated than the ideal parallel plate waveguide. Moreover the mode equations described in the previous section (on ideal parallel plate waveguide) do not hold here because of the anisotropic nature of the ionosphere which allows only the quasi (QTEM, QTE and QTM) modes to exist. To form the mode equation for the Earth-Ionosphere waveguide Budden uses the fact that for a mode to exist in any waveguide the uniform plane waves that constitute the mode must retain their planar fronts upon reflection from the boundaries i.e., the plane wave reflected once from each boundary (the upper and lower) must be in phase with the incident plane wave (Budden, 1961).

The fundamental equation of mode theory which satisfies the mode equation for the Earth-Ionosphere waveguide is given in equation 3-30 shown below:

$$\mathbf{R}_I(\theta)\mathbf{R}_G(\theta) \exp(-2ikh \sin \theta) = \mathbf{I} \quad (3-30)$$

where  $\mathbf{I}$  is the identity matrix. Each angle of incidence  $\theta_i$  that satisfies equation 3-30 defines an individual mode at a certain frequency. The expression for  $\mathbf{R}_I$  is complicated and is difficult to solve analytically. But if the Earth and ionosphere are treated as perfect conductors equation 3-30 would simplify to an equation similar to 3-2).

Another factor that is effected by the nature of the Earth-Ionosphere waveguide is the height gain function described in section 3.4.2 for an ideal parallel plate waveguide. However it can be observed that the height gain functions can be calculated with the knowledge of the mode angles ( $\theta_n$ ) and the reflection coefficients ( $\mathbf{R}_G$  and  $\mathbf{R}_I$ ). The reader is referred to (Pappert and Ferguson, 1986) for a good summary of of the height gain functions that were formulated by Budden. Additionally (Pappert and Ferguson, 1986) also calculate the height gain functions for different source orientations and altitudes and also for different field components. These height gain functions vary depending on the field components, orientation of the dipole and the height of the dipole. These functions contain the modified Henkel functions unlike the sines and cosines as in the ideal parallel plate waveguide. The general equation for the output field  $\mathbf{F}$  with all the factors taken into consideration is given in (Pappert and Ferguson, 1986) and (Cummer, 1997) as:

$$\mathbf{F} = \mathbf{C}(\mathbf{F}) \frac{ik^{\frac{3}{2}} l l}{\sqrt{8\pi x}} \exp\left(\frac{i\pi}{4}\right) \sum \Lambda_{tn} \Lambda_{rn} \exp(-ikx \sin(\theta_n)) \quad (3-31)$$

where  $\mathbf{C}(\mathbf{F})$  is  $\mu_0$  if  $\mathbf{F}$  is a component of the magnetic field and  $\mathbf{C}(\mathbf{F})$  is  $\sqrt{\frac{\mu_0}{\epsilon_0}}$  if  $\mathbf{F}$  is a component of the electric field and  $\Lambda_{tn}$  and  $\Lambda_{rn}$  are called the transmitter and receiver excitation factors respectively, these contain the height gain functions.

The values of  $\Lambda_{tn}$  and  $\Lambda_{rn}$  are derived in (Pappert and Ferguson, 1986) for various orientations of the dipole. For example if an electric dipole is oriented at some angle  $\gamma$  to the z-axis and at an angle  $\phi$  to the direction of propagation (x-axis) at an altitude  $z_t$  (the Earth-Ionosphere waveguide is illustrated in Figure 3-2), the transmitter excitation factor  $\Lambda_{tn}$  is given by (Pappert and Ferguson, 1986) as:

$$\Lambda_{tn} = -\tau_1 \sin(\theta_n) \cos(\gamma) f_1(z_t) + \tau_3 \tau_4 \sin(\gamma) \cos(\phi) f_2(z_t) + \tau \sin(\gamma) \sin(\phi) f_3(z_t) \quad (3-32)$$

where the variables used in the above equation like  $\tau, \tau_1, \tau_3, \tau_4, f_1, f_2$  and  $f_3$  are defined in (Pappert and Ferguson, 1986).

### 3.4.5 Correction for the Curved Nature of the Earth-Ionosphere Waveguide

Another important factor that makes the Earth-ionosphere waveguide substantially different from the ideal parallel plate waveguide is the curved nature of Earth. Especially at large distances (which is the case in this thesis) the curvature of the Earth has a profound effect. In free space the field attenuation due to energy spreading is proportional to  $r^{-1}$ ,  $r$  being the distance from the source. This corresponds to a  $r^{-2}$  factor for the wave power. But for a parallel plate waveguide this spreading factor is reduced to  $r^{-\frac{1}{2}}$  because 'r' now is the 2-d distance from the source (Wood, 2004). For a spherical waveguide of radius 'R' the corresponding attenuation factor would be  $(R \sin(\frac{x}{R}))^{-\frac{1}{2}}$  where 'x' is the great circle distance between the source and the receiver (Budden, 1961). It could be observed that this tends to  $R^{-\frac{1}{2}}$  as  $R \rightarrow \infty$ .

The mode equation given by equation 3–30 must also be modified due to the effect of this curvature because the mode angles are valid only for parallel surfaces and not spherical shells like the Earth. There were a few methods employed in literature to deal with this problem but the most commonly employed method was described in (Richter, 1966). In this paper a co-ordinate transformation method was introduced that converts a cylindrical co-ordinate system into parallel by modifying the refractive index as a gradient  $n_{mod}^2 = \exp(\frac{z}{R})$  so that the rays representing the plane waves bend upwards instead of traveling in straight lines.

### 3.5 Long Wavelength Propagation Capability (LWPC)

LWPC is a collection of FORTRAN programs which enable the implementation of two dimensional waveguide propagation formulation along the great circle path between a transmitter and a receiver. This program applies the implements the concept of propagation of ELF, VLF and LF radio waves to the Earth-ionosphere waveguide, this program sets up the calculation of mode parameters along the selected propagation paths for user defined operating areas (Ferguson and C.H.Shellman, 1989). These set of programs operate separately or in sequence to generate results as per the

requirement of the user. This was developed over many years at the Naval Ocean Systems Center (NCCOSC/NRaD) (Ferguson and C.H.Shellman, 1989). The code has three important parts called PRESEG, MODEFNDR and FASTMC each of which is described below.

### 3.5.1 PRESEG

PRESEG is the FORTRAN program which segments the propagation path between the transmitter and receiver based on the ionospheric, ground and some other parameters, some of which are taken as input. PRESEG determines the necessary waveguide parameters and formats them properly for input to the next stage of the program. Some parameters like magnetic field of Earth, permittivity and conductivity of Earth over the propagation path are taken from built in models and files based on experimental study of these parameters like (Hauser and F.J.Rhoads, 1969). This thesis employs a homogenous ionosphere throughout the entire propagation the details of which are given in the next section. When the inhomogeneities are considered the waveguide is segmented into a number of slabs and slab boundaries are placed where there is a change in the parameters like ionospheric profile, ground conductivity etc (Cummer, 1997).

### 3.5.2 MODEFNDR

MODEFNDR is an important component of the propagation model and is a FORTRAN program which determines the eigen solutions for a horizontally homogenous waveguide/slab (Ferguson and C.H.Shellman, 1989). It takes the waveguide parameters from PRESEG as input and searches for angles inside a predefined region that satisfy the mode condition 3–30. To calculate the necessary mode constants needed for determining the fields in the waveguide, the reflection coefficients for the ionosphere must be solved for a general electron density profile, ion density, collision frequency profile and angle of incidence, this is done by MODEFNDR by assuming that for a fixed angle of incidence the field components vary in x-direction and  $\frac{\partial}{\partial y} = 0$  (Cummer, 1997).

The excitation factors which are needed to determine the final field strengths of each mode are also calculated by this program. The output of this program is given as the input to FASTMC.

### 3.5.3 FASTMC

The propagation path is divided into horizontally homogeneous waveguides/slabs, the signal strength of the electromagnetic field along a path is determined using the mode solutions for each of the homogenous slab by the FASTMC (Ferguson and C.H.Shellman, 1989). FASTMC is a simplified version of another FORTRAN program called FULLMC which is a mathematically rigorous model which does full wave calculations which makes this program quite slow in execution (Ferguson and C.H.Shellman, 1989). This is where FASTMC comes in handy and is an approximate model and runs much faster than the FULLMC and produces comparable results. The output of FASTMC is the magnitude in DB over  $1 \mu\text{V/m}$  field strength and phase in degrees. A correction factor of  $4.1887 \times 10^{-6} \text{I} \exp(i\pi/4)$  must be applied to the output of FASTMC to make it equivalent to a vertical dipole (Cummer, 1997), where I is the current moment of the radiating dipole and f is the frequency.

### 3.5.4 Implementation in LWPC

The fields along a given propagation path in the Earth-Ionosphere waveguide can be calculated using the LWPC code with a set of required parameters given as input. LWPC uses the two dimensional propagational model developed by Budden (Budden, 1961) known as the waveguide mode theory, Figure 3-2 shows the Earth-Ionosphere waveguide. It can be observed from the Figure that the two dimensions are x and z, with x being the direction of propagation along the great circle path and z being the altitude and all the properties of ionosphere and ground assumed to be constant in the y-direction.

There are a set of parameters that need to be input in order to set LWPC to run. These parameters are entered using a model file, after all the required parameters are

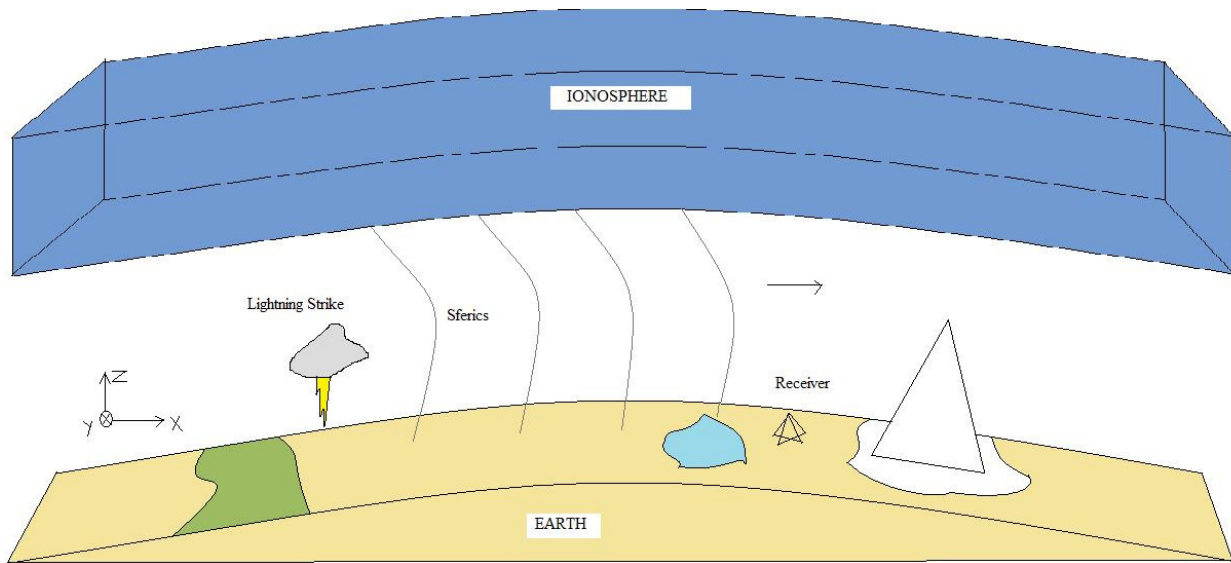


Figure 3-2. Earth-Ionosphere Waveguide

entered it is necessary to give these parameters as inputs to the program PRESEG which itself serves as an input to the programs MODEFNDR and FASTMC. Hence a script is written which inputs the correct parameters in a specified manner to each of the programs and executes them in an orderly manner.

Some parameters which are to be input to the model file and used in this thesis are described below, for a detailed list of various parameters and their default values the reader is referred to ([Dermikol, 1999](#)).

- freq - frequency in KHz, default value is 23.4 KHz
- power - radiated power in Kw, default value is 1 Kw
- trlat, trlong - coordinates of the transmitter in degrees west and degrees north, default values are 158.15°W and 21.41°N respectively
- rlat, rlong - coordinates of receiver in degrees west and degrees north, default values are 0°W and 0°N respectively
- maxalt - highest altitude of the ionospheric profile to be considered for calculation purposes in km, default value is 90 km

- file containing the electron density profiles upto the specified maxalt value
- file containing the information about collision frequency

PRESEG uses the model file with the required parameters and segments the propagation path according to the information in this model file and certain automatic segmentation rules such as the in built conductivity map of Earth and model of Earth's magnetic field , the segmentation information is then stored in output files which are then used by the programs MODEFNDR and FASTMC ([Dermikol, 1999](#)).

MODEFNDR uses the information in the model input file related to electron density profiles and the output from PRESEG to obtain the solution to the mode equation 3–30. To find solutions to the mode equation it needs to calculate the reflection coefficients of the ionosphere and an effective reflection height. It then calculates the attenuation rate, phase velocity, initial excitation, height gain functions for each mode using the values of reflection coefficients.

FASTMC uses the outputs from MODEFNDR and PRESEG to calculate the mode conversion coefficient matrices at different slabs created by PRESEG. Figure 3-3 shows the flowchart pertaining to the execution of LWPC.

### **3.6 Parameters Required to Calculate the Sferic Propagation Model**

As understood from the discussion in the previous section LWPC employs a single-frequency model. To model ELF propagation LWPC solves the time-harmonic propagation problem using the waveguide mode theory of wave propagation ([Budden, 1961](#)). There are certain parameters that need to be calculated as inputs to use the model, parameters like the ground and ambient magnetic field are automatically included in LWPC but certain other parameters like the ionospheric electron density profiles and the Current Moment waveform in the required frequency range which are discussed in the following sections need to be provided.

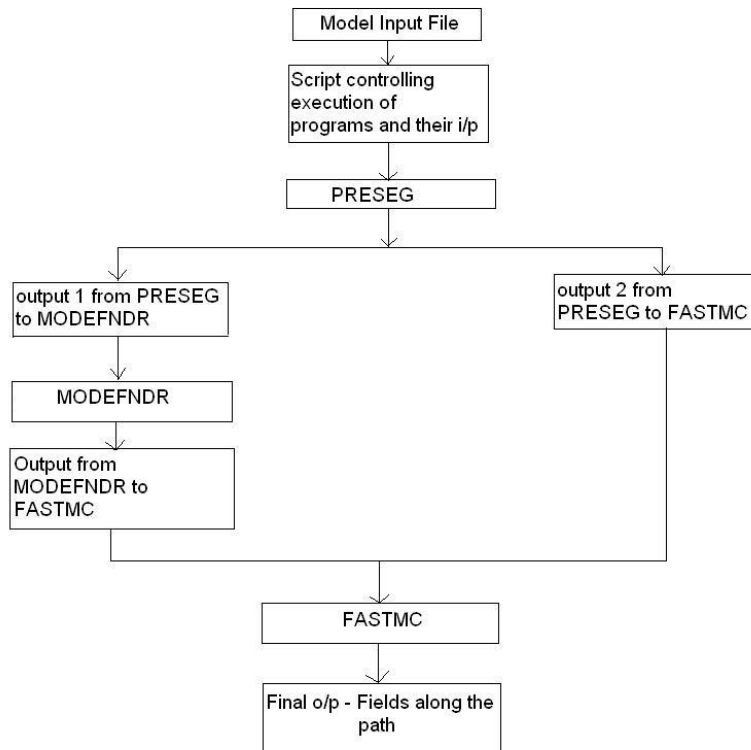


Figure 3-3. Flow chart showing the execution of LWPC

### 3.6.1 Ionospheric Electron Density Profiles

Electron densities at a certain altitude are an important factor in modeling the spheric propagation. The profile was calculated from IRI (International Reference Ionosphere). Though the ionosphere varies from one region to another and from time to time a homogenous ionosphere was assumed through out the propagation path in this thesis. To understand the effects of different ionospheric conditions on spheric propagation four different ionospheric electron density profiles were calculated. Two of the profiles were calculated for daytime ionospheric conditions and two for nighttime ionospheric conditions as shown in Figure 3-4 for altitudes up to 300 km . These profiles were calculated using data from IRI at the coordinates  $0^\circ$  and  $40^\circ$ . One of the daytime ionospheres was at lower electron density values while the other was at higher electron

density values, the nighttime ionospheres differ by the fact that one of them has a valley at 100-150 Km while the other does not. The valley occurs at the E-region of the nighttime ionosphere due to the decrease in electron density values and is a common phenomena at nights.

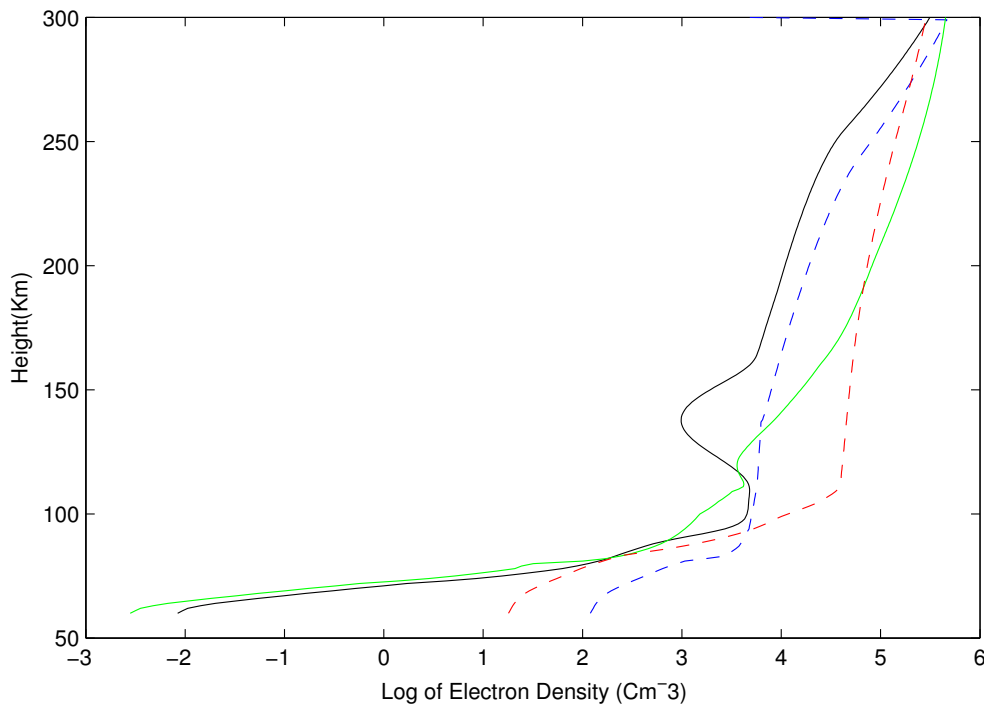


Figure 3-4. Representative electron density profiles

The International Reference Ionosphere ([Bilitza, 2001](#)) is an international project sponsored by the Committee on Space Research (COSPAR) and the International Union of Radio Science (URSI). IRI gets its data from Ionosodes, Alouette topside sounders, Incoherent Scatter Radars and in situ instruments on several satellites and rockets. It is the international standard for terrestrial ionosphere since 1999.

### 3.6.2 Current Moment Waveform of a Lightning Strike

The other parameter that is needed to model the ELF spheric propagation using LWPC is current moment waveform in the required frequency range. As mentioned in the previous sections the LWPC gives a time-harmonic (single frequency) solution and

so it is required to get the current moment waveform as a function of frequency (i.e., in frequency domain).

Previous theoretical studies of ELF sferics (Cummer, 1997),(S.A.Cummer and U.S.Inan, 2000) etc have assumed an ideal impulse lightning discharge and modeled the corresponding current moment waveform. Although this is a decent approximation there are certain spectral features which cannot be modeled theoretically and moreover every lightning strike differs from the other. This makes it difficult to model sferics accurately. In this work the sferics radiated from rocket triggered lightning are being modeled, the advantage with rocket triggered lightning is the availability of very accurate data about the lightning.

Figure 3-5 shows the current waveform that has been used in this thesis. It represents the current flowing at the base of the lightning channel during the rocket triggered lightning experiment conducted at Camp Blanding on 29<sup>th</sup> March 2009.

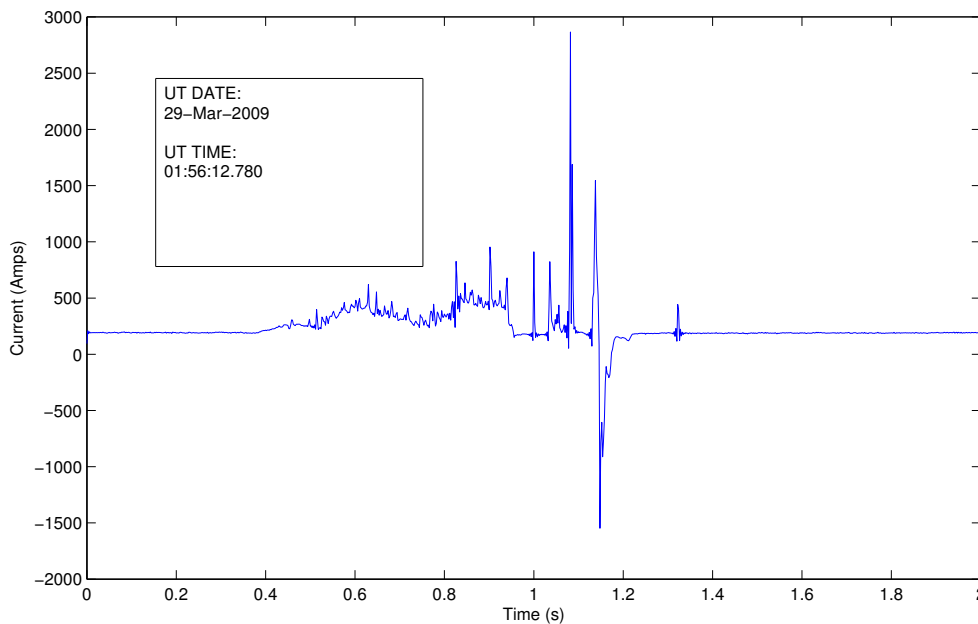


Figure 3-5. Current vs Time waveform from rocket triggered lightning

The height of the lightning channel is assumed to be 7.5 Km in this work.

## CHAPTER 4 MODELING ELF SFERICS

This chapter describes the modeling of ELF sferics after all the required input parameters discussed in the previous chapter are gathered. All the modeling work presented in this chapter is done using a set of computer programs called LWPC which is based on a single frequency propagation model (Budden, 1961). First the sferics are modeled assuming a homogeneous ground and a homogeneous ionosphere throughout the propagation path and then a more complicated case with an inhomogeneous ground profile is considered.

The model completes its calculations in the frequency domain and the output is a spectrum of the sferic as a function of frequency. The only mode propagating is the QTEM mode which does not have a cut-off frequency and the attenuation rate as a general trend increases steadily with the frequency (although certain exceptions were observed at some frequencies) causing the mode to die off eventually at around 1.7 KHz.

### 4.1 Homogeneous Waveguide

ELF sferics in the range of frequencies 10-500 Hz (with the difference between each frequency sample being 10 Hz) are modeled assuming a homogeneous ground profile of conductivity  $10^{-2}$  S/m and a relative permittivity of 15. A nighttime ionospheric profile shown in Figure 4-1 is taken and is assumed to be homogeneous throughout the propagation path, three different propagation paths of distances 1000 km, 2000 km and 3000 km are considered. An impulse lightning current waveform similar to the one used in (Cummer, 1997) and (S.A.Cummer and U.S.Inan, 2000) is employed here, this case is similar to the modeling presented in (S.A.Cummer and U.S.Inan, 2000).

The spectrum shown in Figure 4-2 are the amplitudes of transverse horizontal magnetic field  $B_y$  at the specified distances. It can be observed that the results presented are similar to the ones obtained in (S.A.Cummer and U.S.Inan, 2000) for

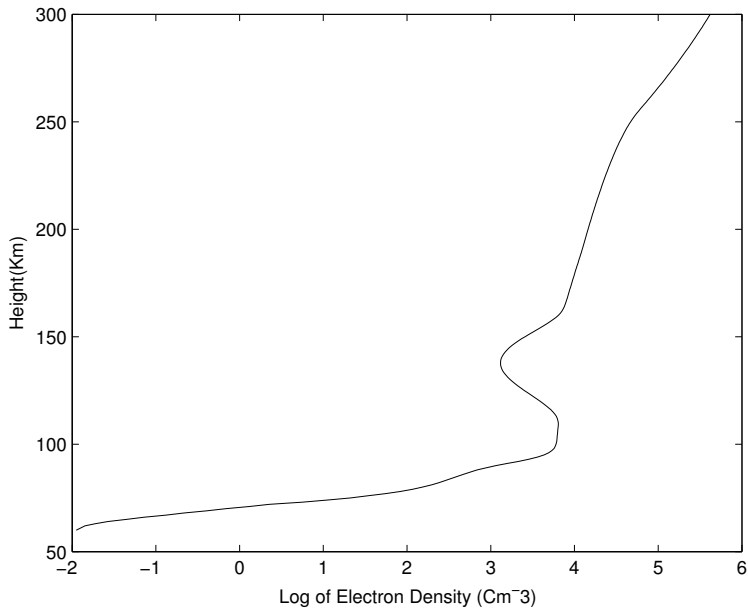


Figure 4-1. Representative nighttime ionosphere

the nighttime ionosphere. Figure 4-3 shows the same spectrum shown in Figure 4-2 in decibel scale.

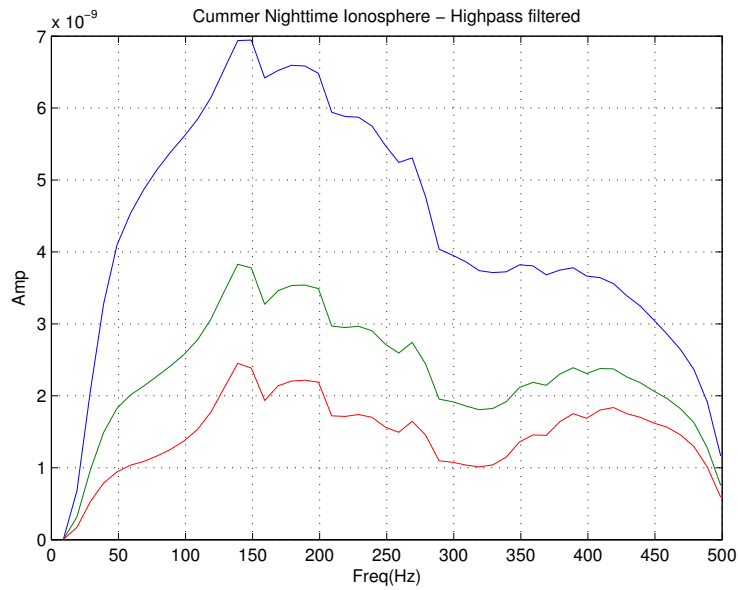


Figure 4-2. ELF spheric spectra of homogeneous ground in linear scale

The spectra are passed through a high-pass filter of cut-off frequency 30 Hz.

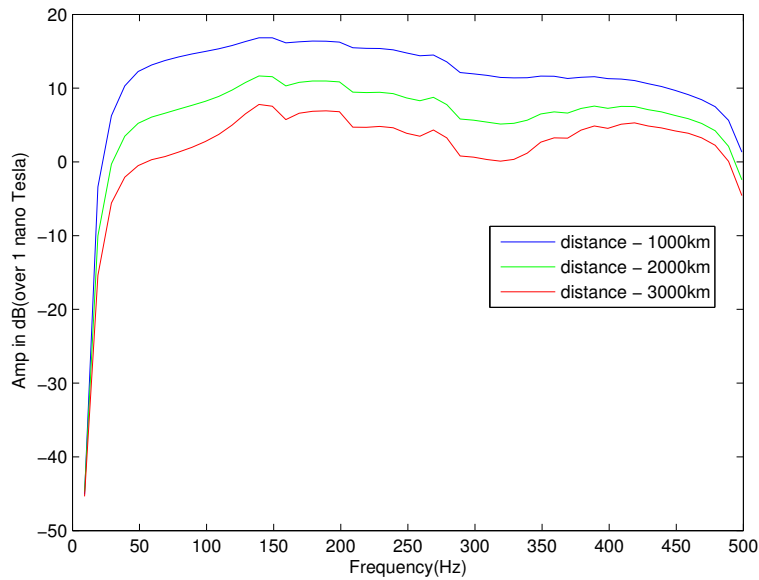


Figure 4-3. ELF spheric spectra of homogeneous ground in decibel scale

## 4.2 Inhomogeneous Ground

In this case a inhomogeneous ground is considered with conductivity varying from  $10^{-2}$  to  $10^{-3}$  S/m. The rest of the input parameters are the same as those assumed in the previous case and an arbitrary propagation path of distance around 2000 Km is considered. The ELF spectra are modeled in the frequency range of 10-500 Hz (with the difference between each frequency sample being 1Hz)

The spectra are passed through a high-pass filter of cut-off frequency 30 Hz in a manner similar to the previous case. The Figure 4-4 shows the amplitude of transverse horizontal magnetic field  $B_y$  computed compared with the amplitude calculated in the previous case for a homogeneous ground covering a distance of 2000Km. Figure 4-5 shows the comparison of amplitudes of the two spectra in decibel scale.

It could be observed that the results obtained in both the cases are similar except for some differences like the amplitude of spectra calculated assuming an inhomogeneous ground is less than the amplitude calculated using homogeneous ground, this assumption is valid only for short distances which have a fairly similar

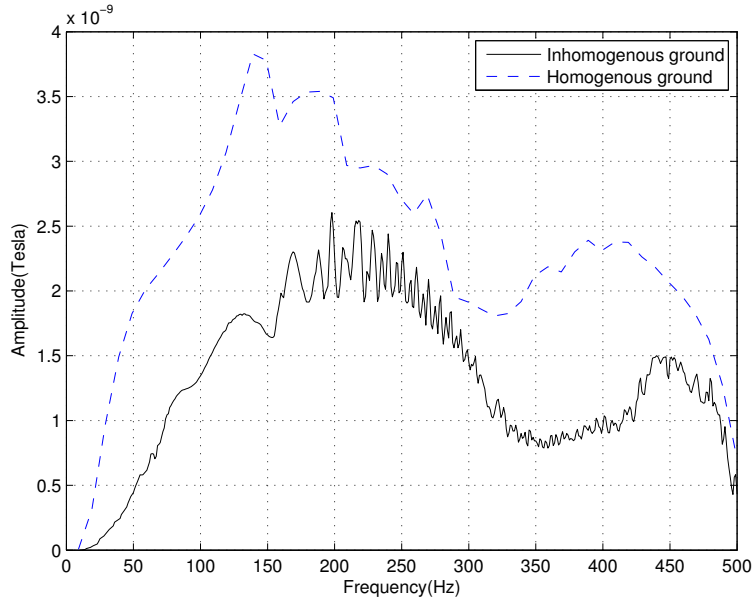


Figure 4-4. Comparison of ELF spheric spectra for inhomogeneous and homogeneous ground (distance-2000Km)

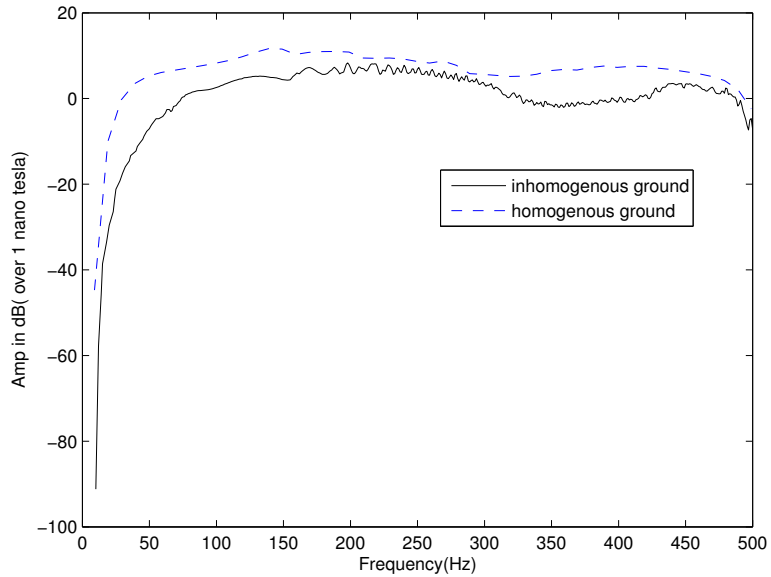


Figure 4-5. Comparison of ELF spheric spectra for inhomogeneous and homogeneous ground (distance-2000Km) in decibel scale

ground throughout the propagation path and this approximation does not produce accurate results when the propagation path has huge variations in conductivity due to the presence of both land and sea in the propagation path. Such a situation is dealt in the next section.

### **4.3 Modeling of ELF sferics Propagating from Camp Blanding to McMurdo Station**

In this case a complicated inhomogeneous ground is considered. The source of the sferic- the lightning discharge is at Camp Blanding, Florida ( $29.94^{\circ}N$  and  $-82.03^{\circ}W$ ) and the receiver is at McMurdo Station, Antarctica ( $-77.88^{\circ}N$  and  $166.73^{\circ}W$ ) with a total propagation distance of 13740 Km. The electron density values specified in the previous chapter are used and the effect of ions is neglected. The source current moment waveform presented in the previous chapter is used assuming a vertical dipole discharge. LWPC calculates the amplitude and phase for any orientation of the hertzian dipole, to make the sferic waveform equivalent to that caused due to the lightning discharge used in this thesis, the output of LWPC should be convolved with the current-moment waveform, to do that the current-moment waveform was converted into frequency domain and it was multiplied with the output of LWPC in linear scale.

The current waveform is taken from the rocket triggered lightning conducted at Camp Blanding, thereby giving more realistic waveform compared to some previous models (Cummer, 1997) which use theoretically modeled return stroke of lightning. The lightning discharge used in the calculations presented in this thesis occurred on March 29, 2008.

The sferic spectra calculated in this thesis are in the frequency band of 45-500Hz assuming an inhomogeneous ground with conductivity varying from  $10^{-4}$  to 4 S/m and a homogeneous ionosphere throughout the propagation path. Figure 4-6 shows the great circle path of propagation of the sferic from Florida to Antarctica.

The output calculated from LWPC exhibited some sudden jumps with the change in conductivity of the ground. This phenomenon could not be explained in this thesis and the output of LWPC was adjusted manually such that the variation of amplitude with distance looked smooth without sudden jumps, this is shown more clearly in the next chapter. The spheric waveforms shown in this thesis were calculated assuming a Hermitian symmetry (S.A.Cummer and U.S.Inan, 2000).

All the plots corresponding to the same ionosphere are in the same color, with black representing nighttime ionosphere with a valley, blue representing daytime ionosphere type1, green representing nighttime ionosphere without a valley and red representing daytime ionosphere type 2.



Figure 4-6. Propagation Path of the Spheric from Florida to Antarctica (Great Circle)

Four different ionospheres shown in the previous section are considered in this case.

### 4.3.1 Nighttime Ionosphere With a Valley

Figure 4-7 below shows the nighttime ionosphere with a valley at 100-150 km. The valley is the region of the ionosphere where there is a decrease in the electron density values compared to other regions of the ionosphere.

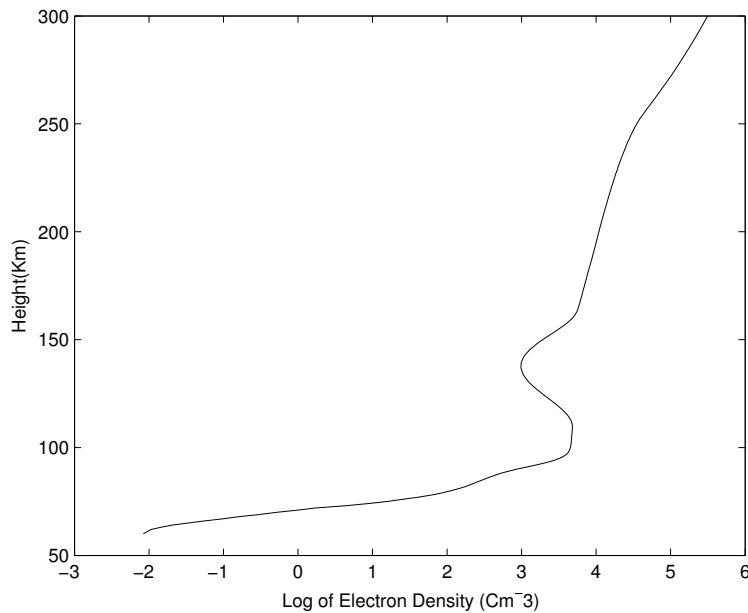


Figure 4-7. Nighttime ionosphere with a valley

Figure 4-26 shows the current waveform employed here in calculating the spheric spectrum and waveform, the current waveform as observed is for a time-period of one second.

Figure 4-9 shows the direct output of LWPC without convolving it with lightning current moment waveform.

The valley usually occurs in the E-region of the ionosphere at a height of 100-150 Km, this region of the ionosphere has a significant affect on the spheric waveform. Figure 4-10 shows the spectrum of  $B_y$  that would be observed at the receivers in a decibel scale and Figure 4-11 shows the spectrum of the spheric ( $B_y$ ) in a linear scale (Tesla),

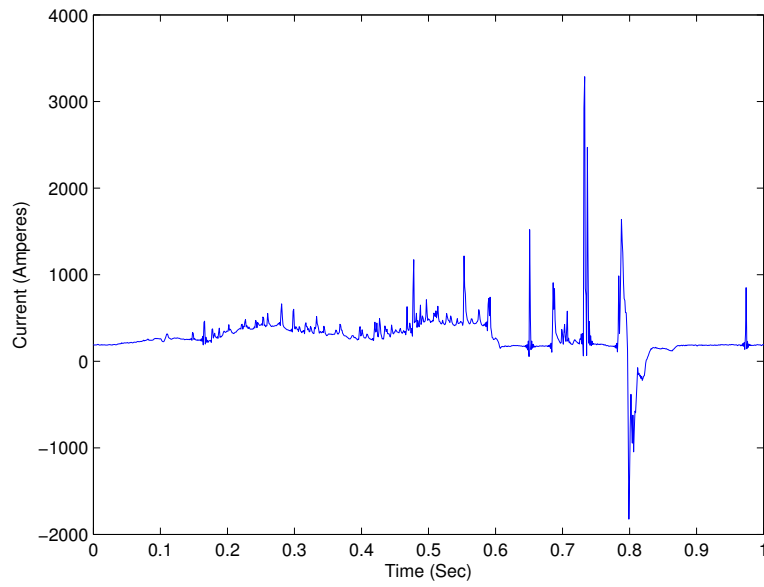


Figure 4-8. Current Waveform employed in calculations

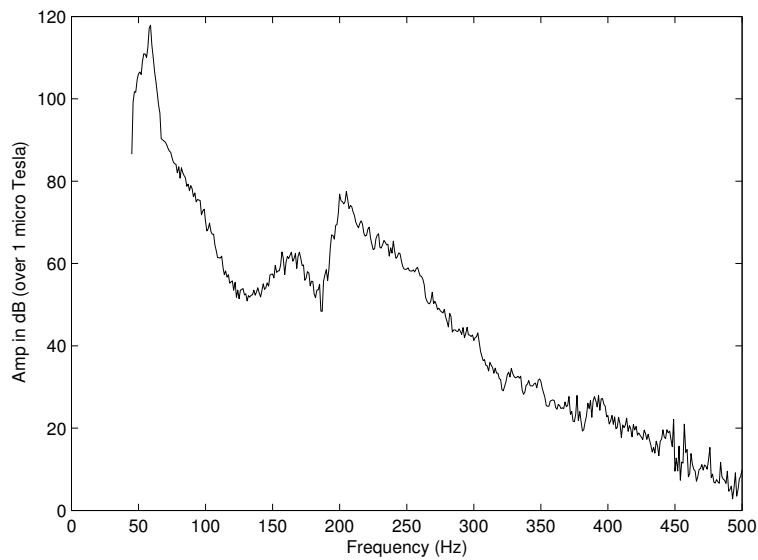


Figure 4-9. LWPC output for nighttime ionosphere with a valley

it could be observed from Figure 4-10 that this region produces certain resonance like effects and the waveform is a little complicated compared other waveforms discussed in the subsequent sections.

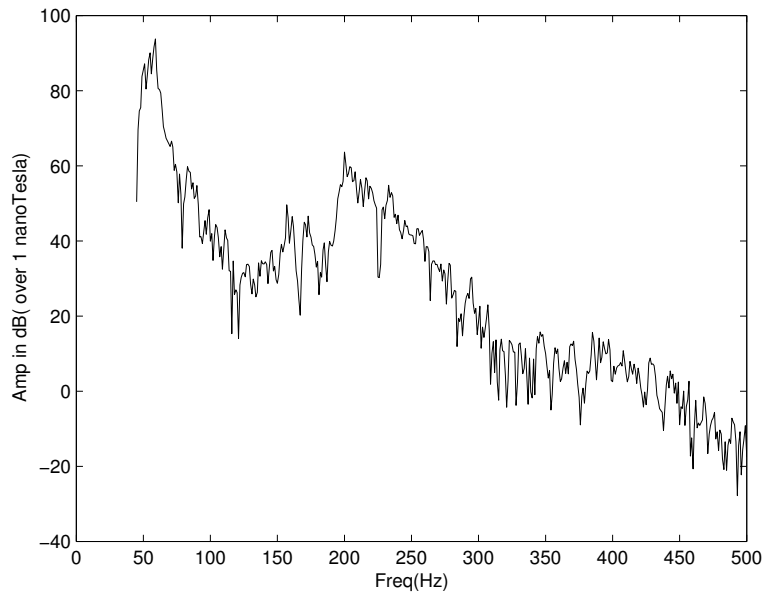


Figure 4-10. Modeled ELF spectrum in decibel scale (over 1 nanotesla) for nighttime ionosphere with a valley

Figure 4-12 shows the sferic waveform (the time domain signal) for the nighttime ionosphere considered in this section.

#### 4.3.2 Daytime Ionosphere - Type 1

Figure 4-13 shows the daytime ionospheric electron density values. The daytime ionosphere is not very complicated compared to the nighttime ionosphere.

Figure 4-26 shows the current waveform employed here in calculating the sferic spectrum and waveform, the current waveform as observed is for a time-period of one second.

Figure 4-15 shows the direct LWPC output for this ionosphere without convolving it with current moment waveform.

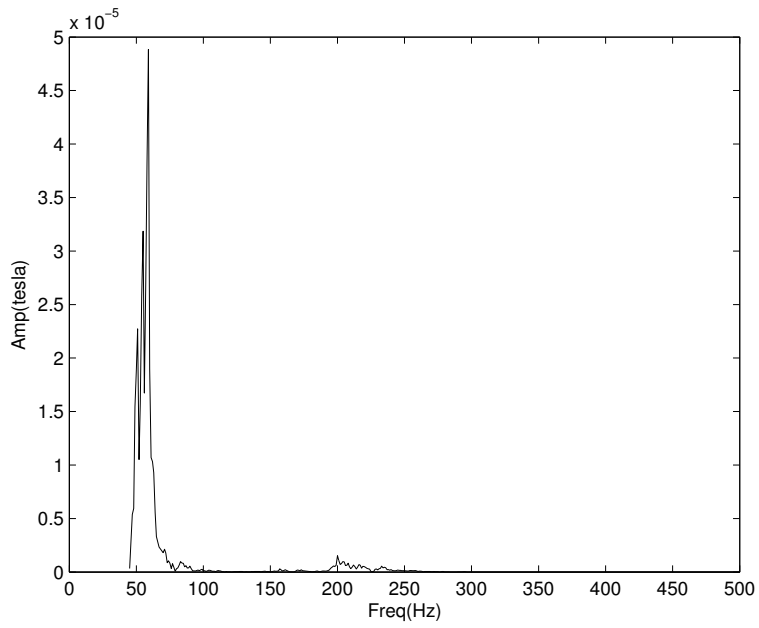


Figure 4-11. Modeled ELF spectrum in linear scale for nighttime ionosphere with a valley

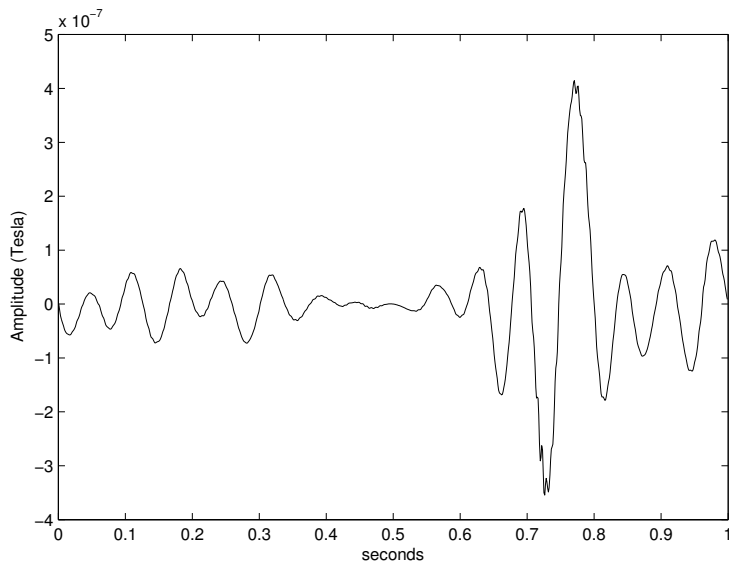


Figure 4-12. Modeled ELF spheric waveform for nighttime ionosphere with a valley

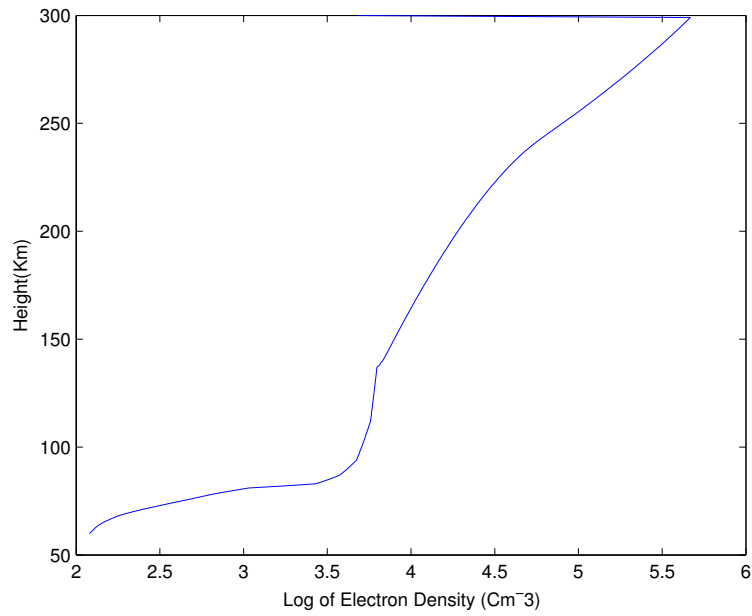


Figure 4-13. Daytime ionosphere Type 1

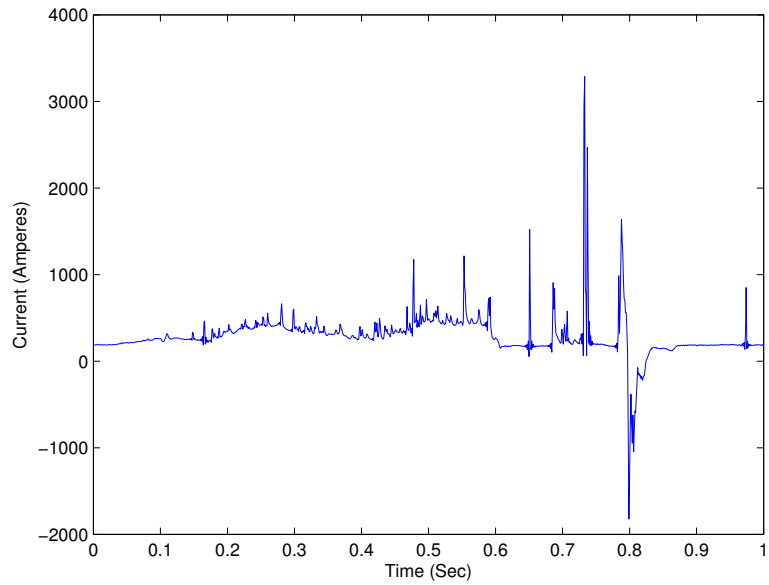


Figure 4-14. Current Waveform employed in calculations

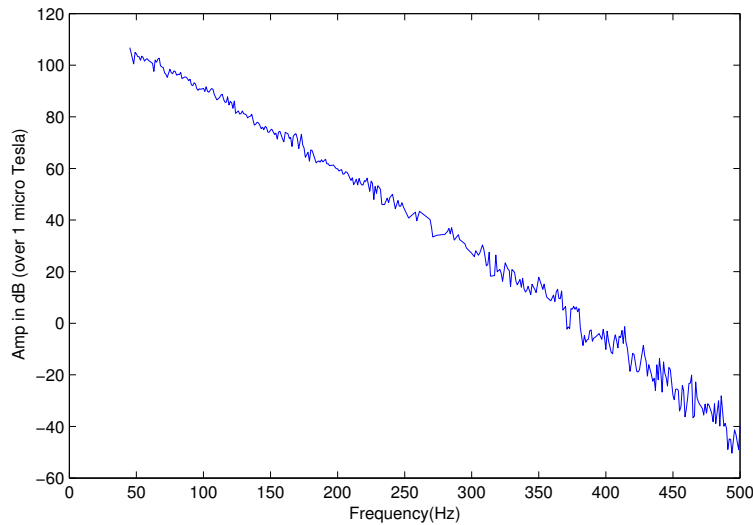


Figure 4-15. LWPC output for daytime ionosphere type 1

Figure 4-16 shows the spectrum of  $B_y$  that would be observed at the receivers in a decibel scale and Figure 4-17 shows the spectrum of the sferic ( $B_y$ ) in a linear scale (Tesla) for the daytime ionosphere, the sferics obtained from daytime ionosphere is not as complicated as the nighttime ionosphere with a valley, with the amplitude decreasing with increase in frequency. Figure 4-18 shows the sferic waveform for this spectrum.

### 4.3.3 Nighttime Ionosphere Without a Valley

Figure 4-7 below shows the nighttime ionosphere without a valley at 100-150 km.

Figure 4-26 shows the current waveform employed here in calculating the sferic spectrum and waveform, the current waveform as observed is for a time-period of one second.

Figure 4-21 shows the direct LWPC output for the ionosphere shown in the previous figure without convolving it with current moment waveform.

Unlike the previous nighttime ionosphere this ionosphere has no valley. Figure 4-10 shows the spectrum of  $B_y$  that would be observed at the receivers in a decibel scale and Figure 4-11 shows the spectrum of the sferic ( $B_y$ ) in a linear scale (Tesla), it could be observed from Figure 4-10 that there are no resonance like phenomena as observed

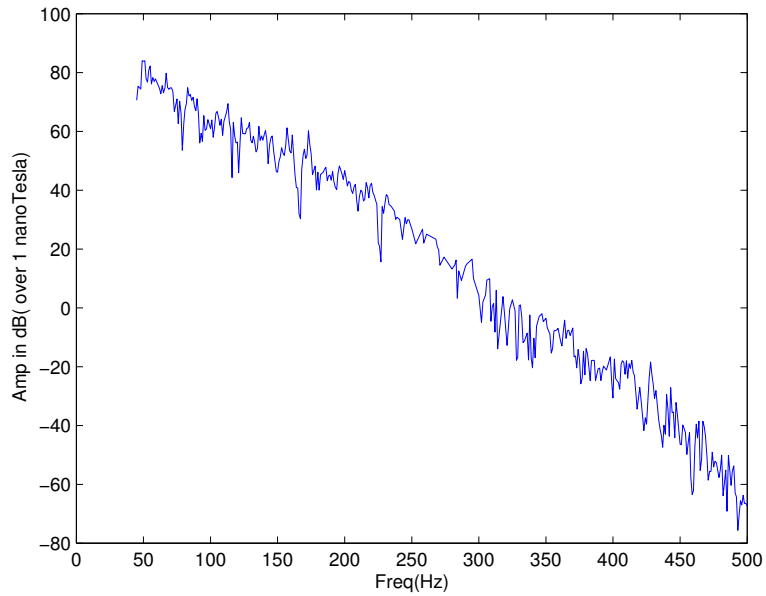


Figure 4-16. Modeled ELF spectrum waveform in decibel scale (over 1 nanotesla) for daytime ionosphere type 1

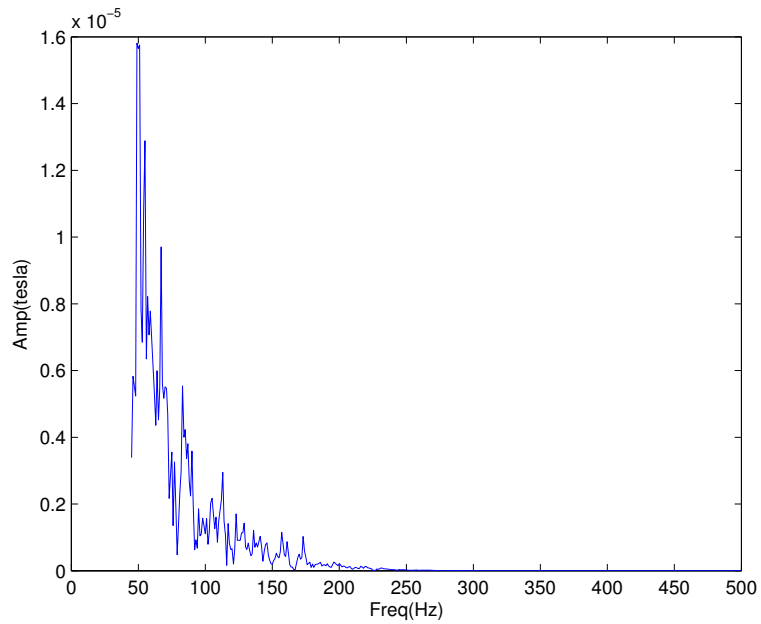


Figure 4-17. Modeled ELF spectrum in linear scale for daytime ionosphere type 1

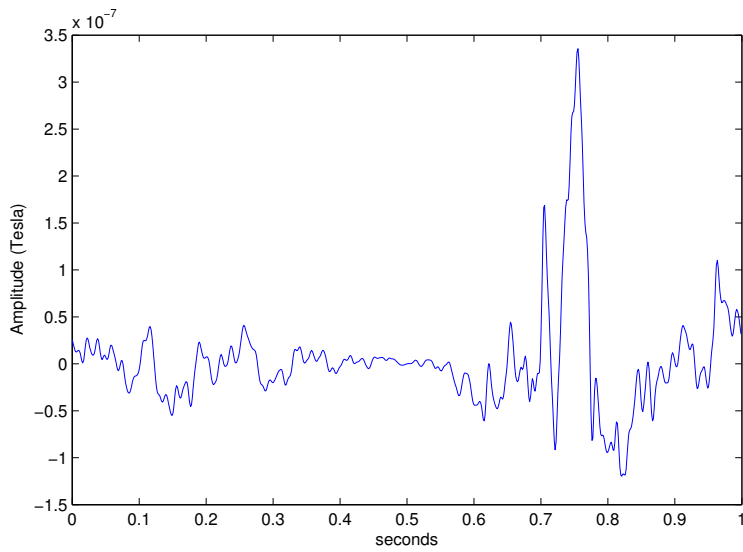


Figure 4-18. Modeled ELF spheric waveform for daytime ionosphere type 1

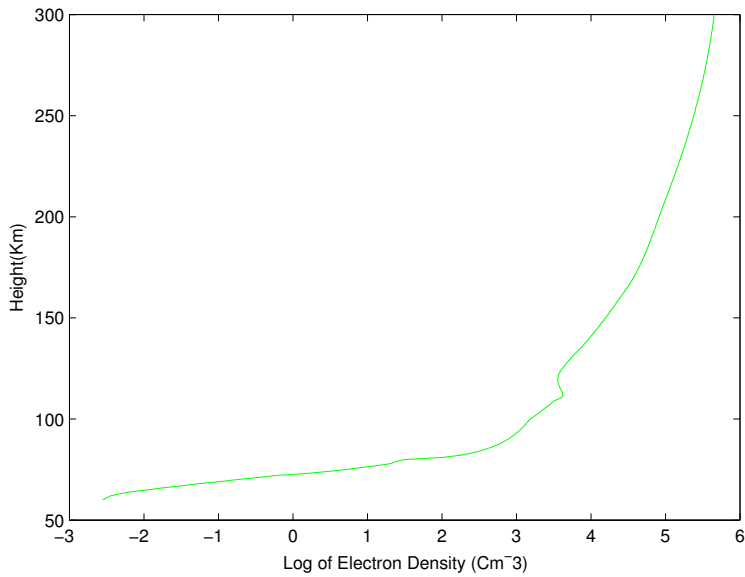


Figure 4-19. Nighttime ionosphere without a valley

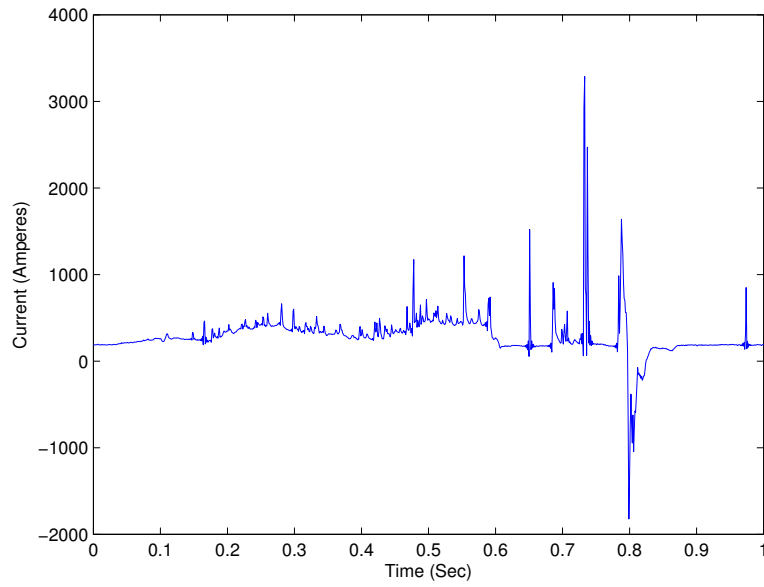


Figure 4-20. Current Waveform employed in calculations

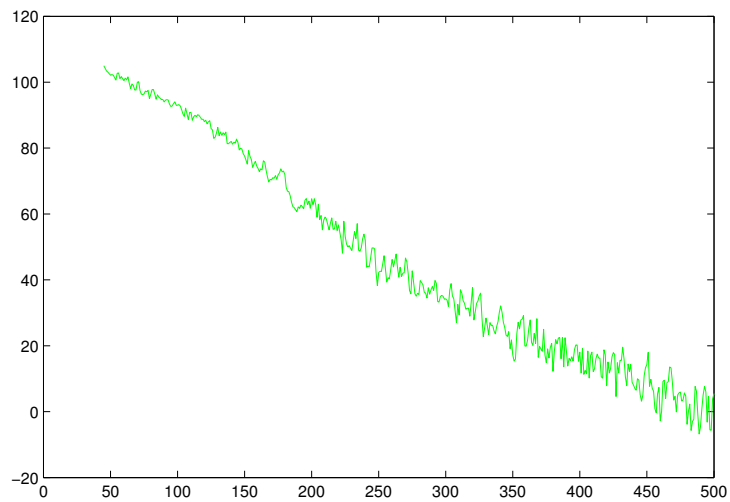


Figure 4-21. LWPC output for nighttime ionosphere without a valley

in the previous nighttime ionosphere (with the valley), thus showing the valley has a great impact on the shape of the spheric. Figure 4-24 shows the spheric waveform for the spectrum calculated in this section.

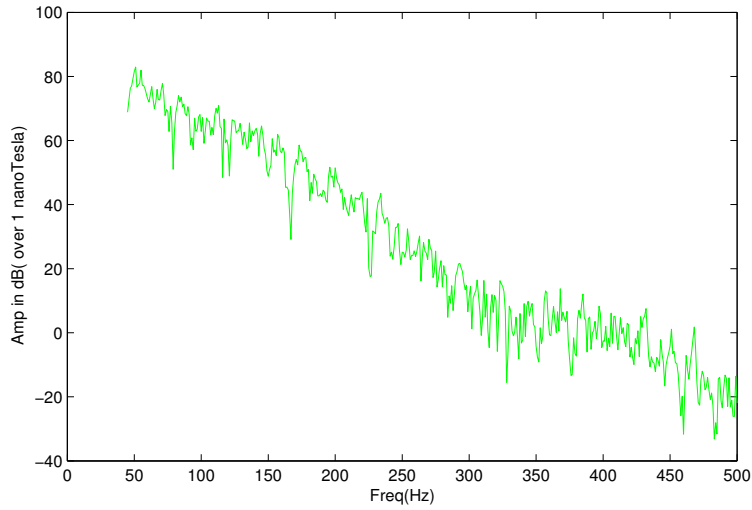


Figure 4-22. Modeled ELF spectrum in decibel scale (over 1 nanotesla) for nighttime ionosphere without a valley

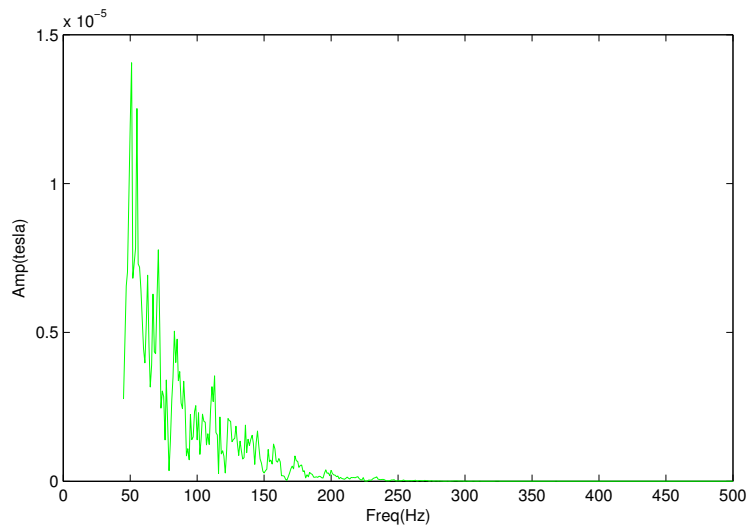


Figure 4-23. Modeled ELF spectrum in linear scale for nighttime ionosphere without a valley

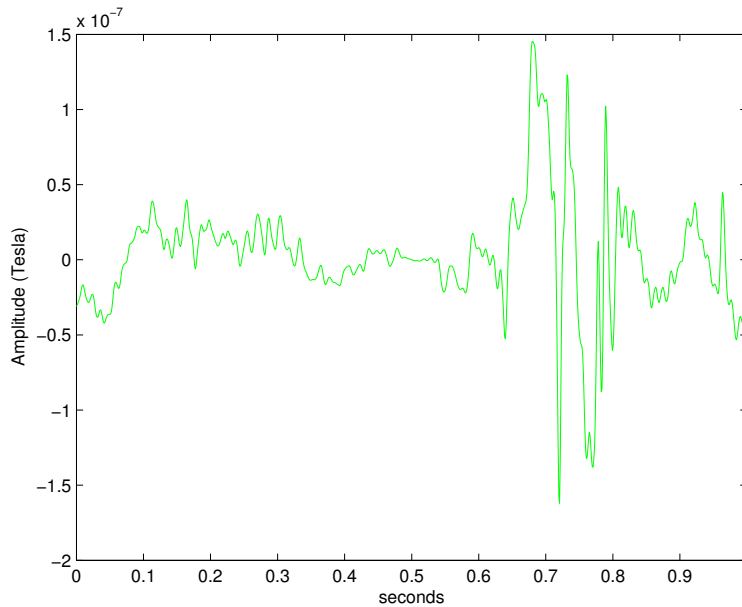


Figure 4-24. Modeled ELF spheric waveform for nighttime ionosphere without a valley

#### 4.3.4 Daytime Ionosphere - Type 2

Figure 4-25 shows the daytime ionospheric electron density values, this ionosphere has higher electron density values compared to the previous daytime ionosphere discussed in the previous section.

Figure 4-26 shows the current waveform employed here in calculating the spheric spectrum and waveform, the current waveform as observed is for a time-period of one second.

Figure 4-27 shows the direct LWPC output for this ionosphere without convolving it with current moment waveform.

Figure 4-28 shows the spectrum of  $B_y$  that would be observed at the receivers in a decibel scale and Figure 4-17 shows the spectrum of the spheric ( $B_y$ ) in a linear scale (Tesla) for the daytime ionosphere (with higher electron density values), the spherics obtained from this ionosphere are somewhat lower in amplitude than the previous daytime ionosphere which could be attributed to the higher electron density

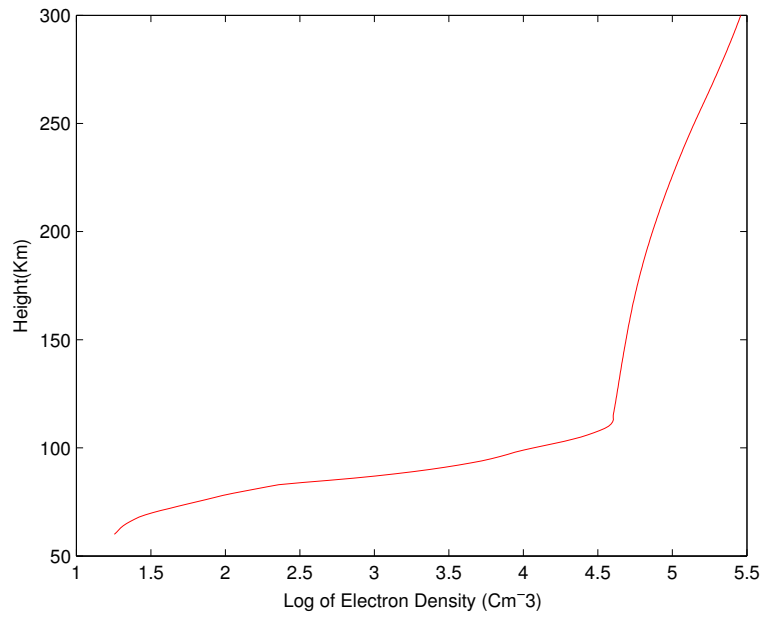


Figure 4-25. Daytime ionosphere Type 2

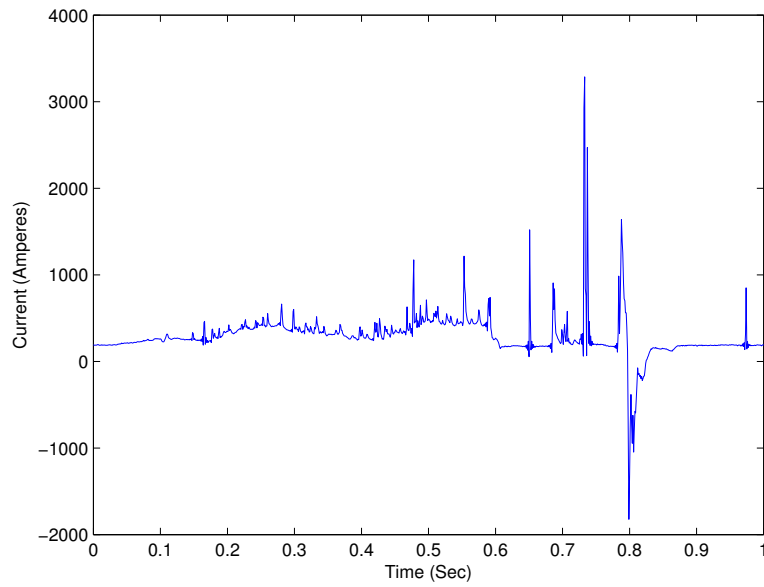


Figure 4-26. Current Waveform employed in calculations

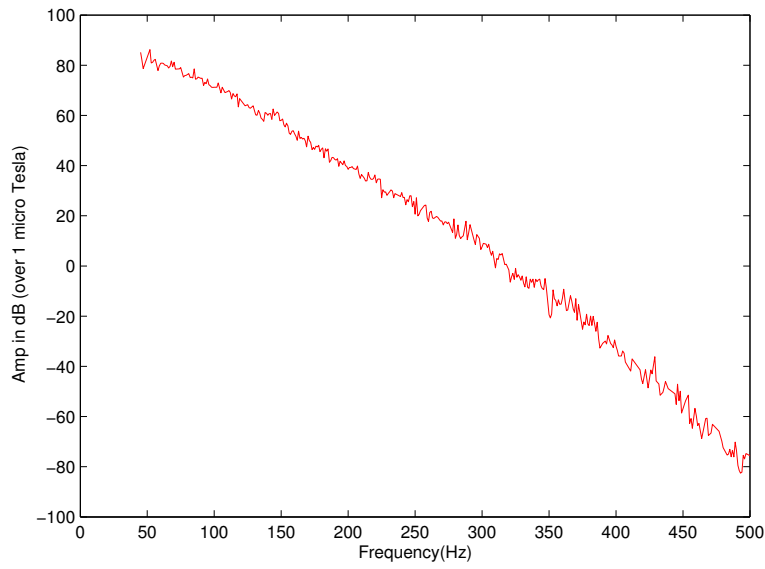


Figure 4-27. LWPC output for daytime ionosphere type 2

values. Figure 4-30 shows the sferic waveform for the spectra calculated using daytime ionosphere type 2.

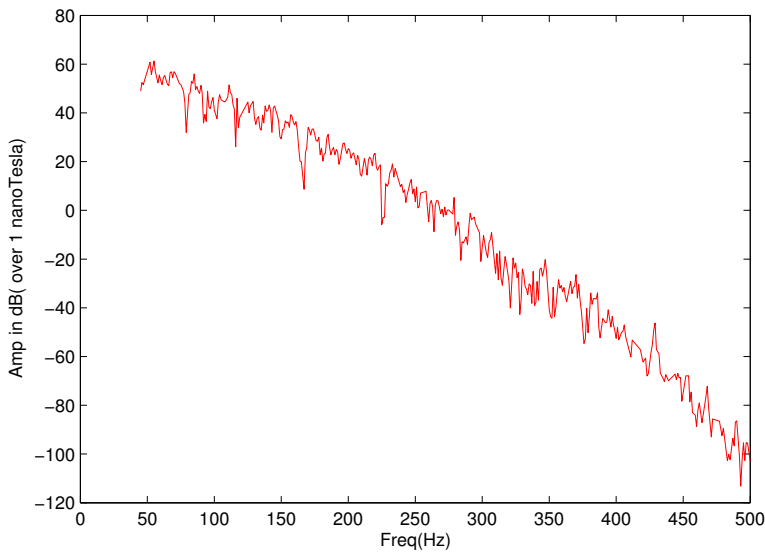


Figure 4-28. Modeled ELF spectrum in decibel scale (over 1 nanotesla) for daytime ionosphere type 2

Thus it could be observed from the above spectra that ionosphere plays a significant role in determining the shape of the sferic spectrum, more importantly it

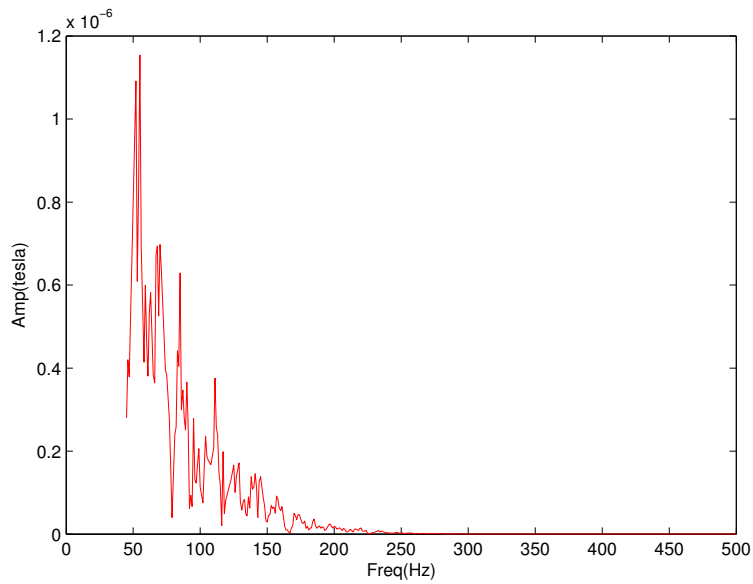


Figure 4-29. Modeled ELF spheric waveform in linear scale for daytime ionosphere type 2

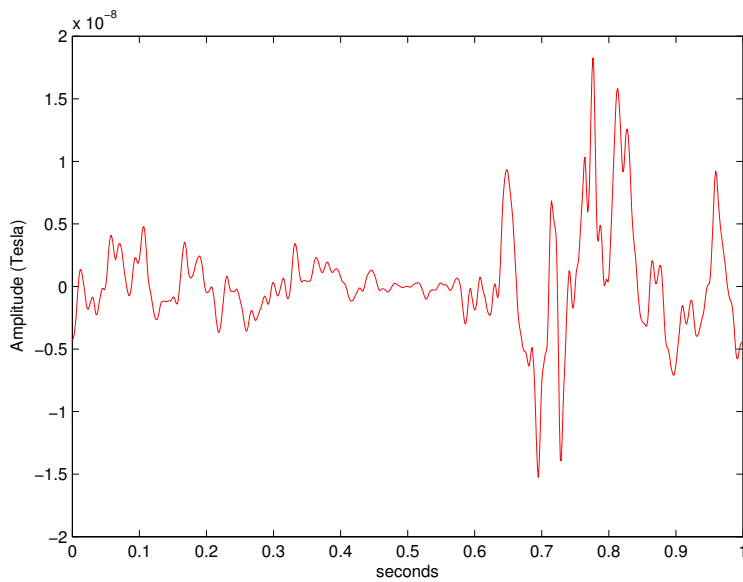


Figure 4-30. Modeled ELF spheric waveform for daytime ionosphere type 2

is the E-region of the ionosphere that plays a significant role unlike for the VLF waves where the D-region of the ionosphere plays a vital role (Cummer, 1997). This data could be used to determine the noise floor of the receivers that are used in Antarctica to detect the sferics.

#### 4.4 Effects of Different Components of Current on the Sferic Waveform

This section deals with the effects of different components of current on the sferic waveform, to do that the current waveform is passed through different rectangular windows each of which selects a particular component and removes the other components by making them zero. By doing this the time period of the current waveform still remains the same but only the selected component remains and the rest of the waveform becomes zero.

Figure 4-31 shows the different components of the current waveform used in this thesis, it could be seen from the figure that this particular current waveform has an Initial Continuous Current (ICC) phase followed by five return strokes.

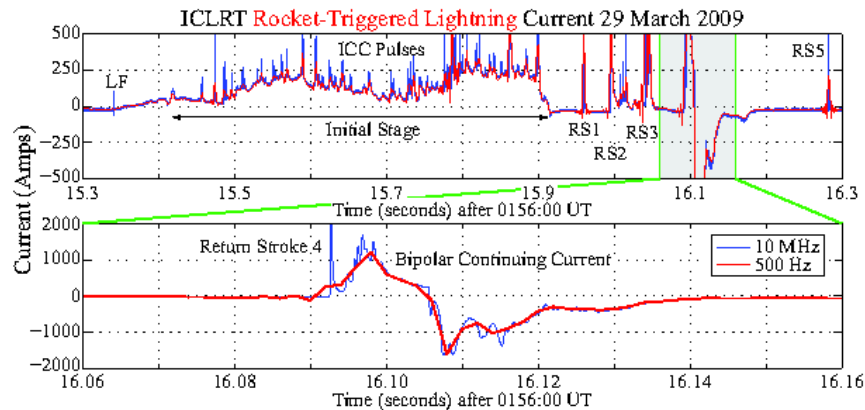


Figure 4-31. Components of the Current Waveform Used

Each of these components are convolved with LWPC such that only the effects of that particular component are observed, the figures below show each of the component

of current and its resultant sferic waveform for nighttime ionosphere with a valley as an example.

Figure 4-32 shows the ICC component of the current and Figure 4-33 shows the resultant sferic waveform.

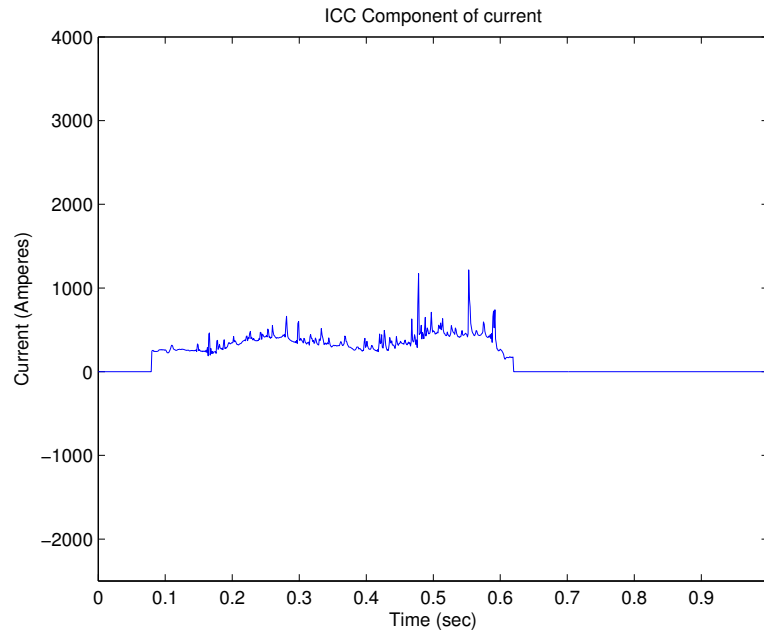


Figure 4-32. ICC Component of the Current Waveform Used

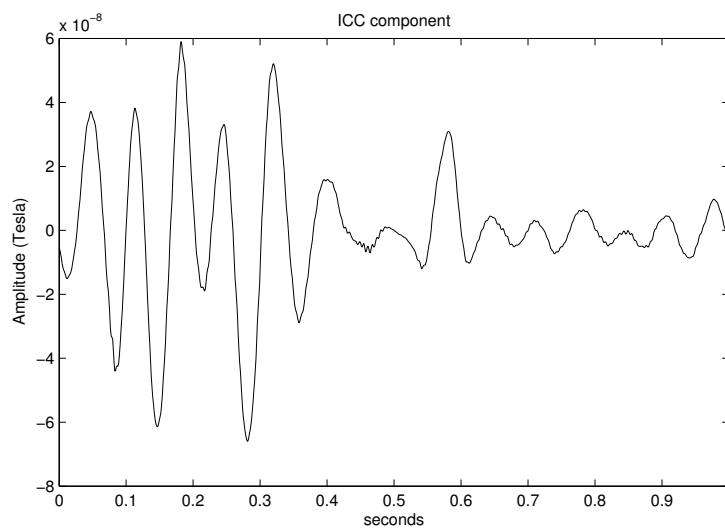


Figure 4-33. Resultant Sferic Caused due to the ICC Component of Current

Figure 4-34 shows the return stroke 1 of the current and Figure 4-35 shows the resultant sferic waveform.

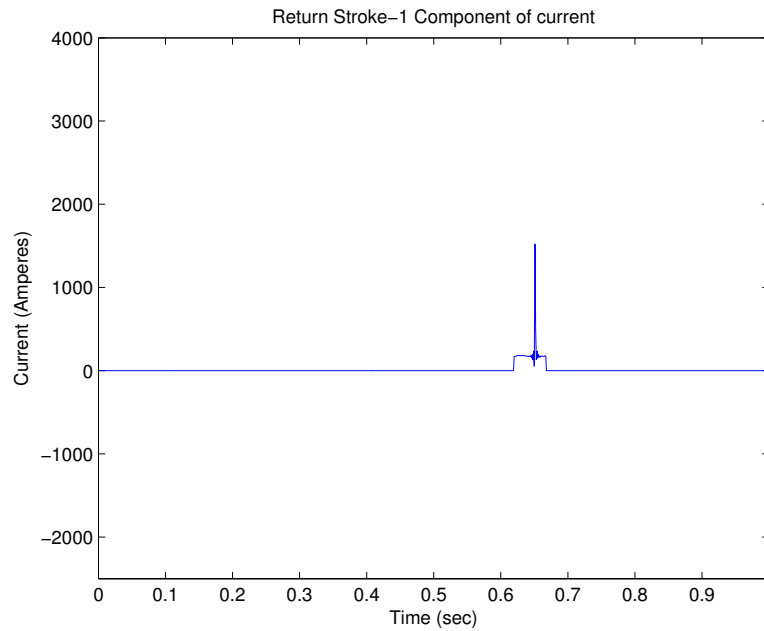


Figure 4-34. Return Stroke 1 of the Current Waveform Used

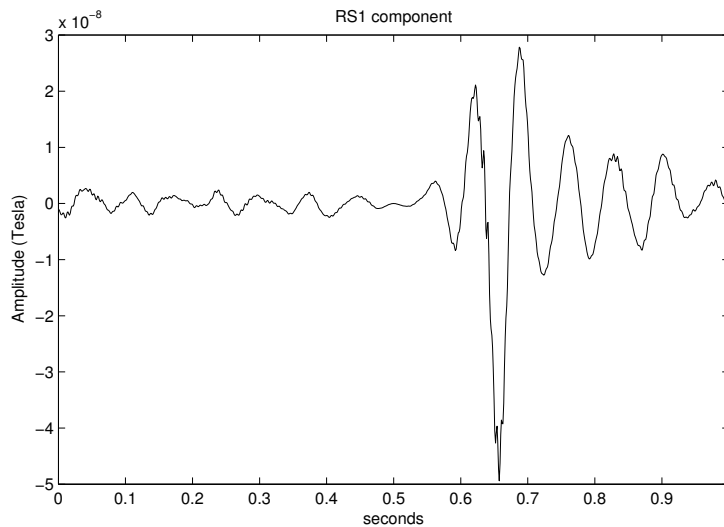


Figure 4-35. Resultant Sferic Caused due to the Return Stroke 1 of Current

Figure 4-36 shows the return stroke 2 of the current and Figure 4-37 shows the resultant sferic waveform.

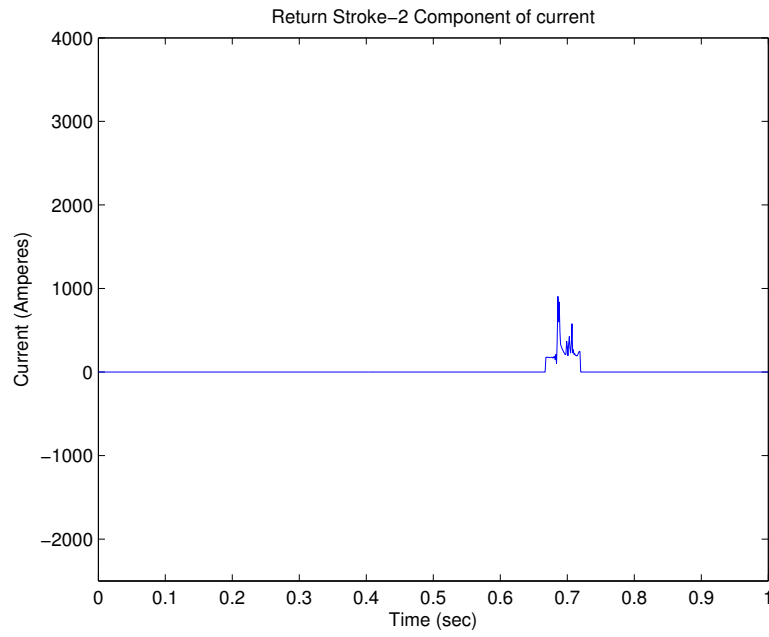


Figure 4-36. Return Stroke 2 of the Current Waveform Used

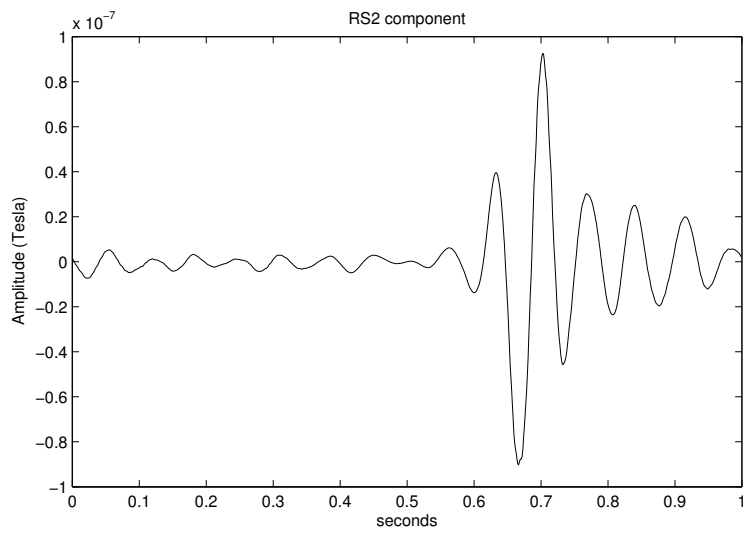


Figure 4-37. Resultant Sferic Caused due to the Return Stroke 2 of Current

Figure 4-38 shows the return stroke 3 of the current and Figure 4-39 shows the resultant sferic waveform.

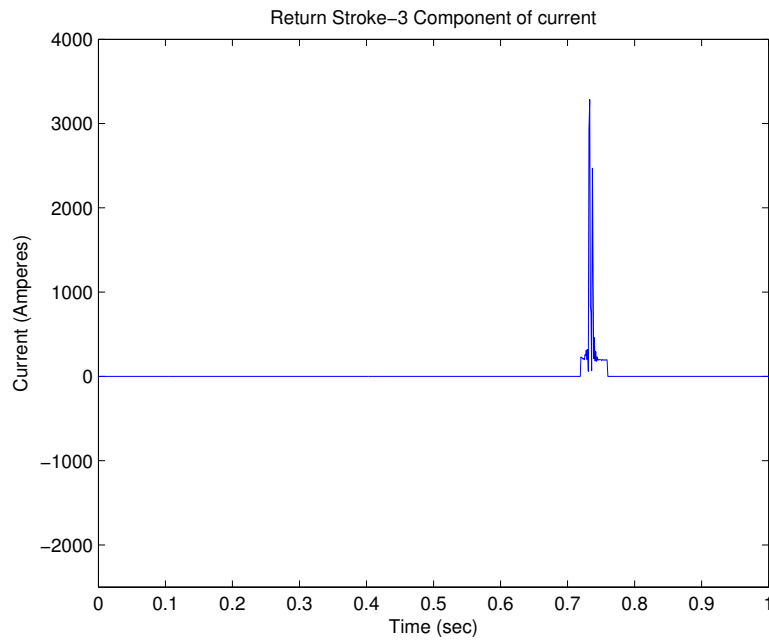


Figure 4-38. Return Stroke 3 of the Current Waveform Used

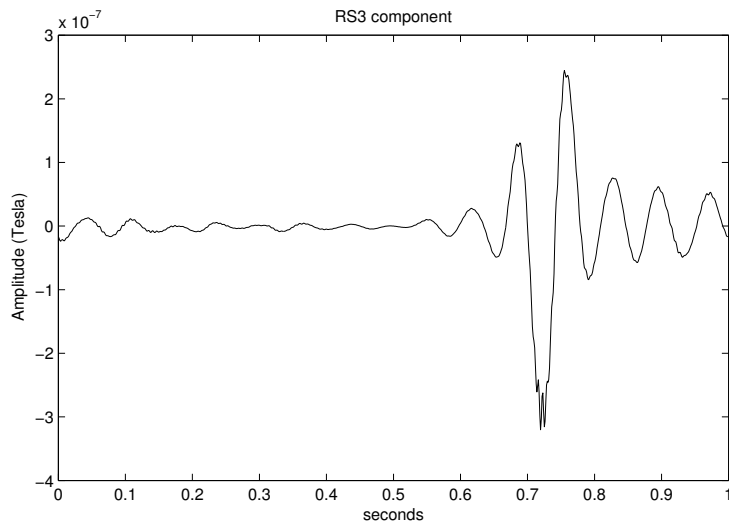


Figure 4-39. Resultant Sferic Caused due to the Return Stroke 3 of Current

Figure 4-40 shows the return stroke 4 of the current and Figure 4-41 shows the resultant sferic waveform.

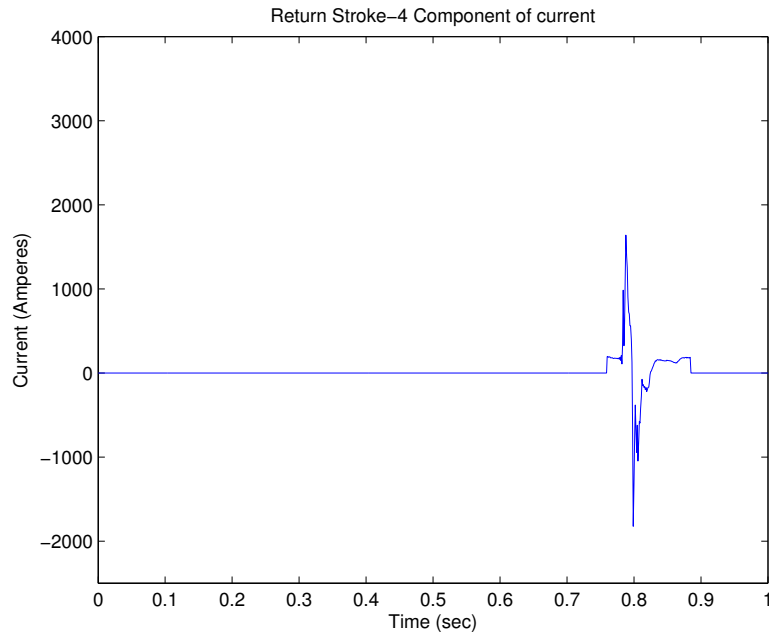


Figure 4-40. Return Stroke 4 of the Current Waveform Used

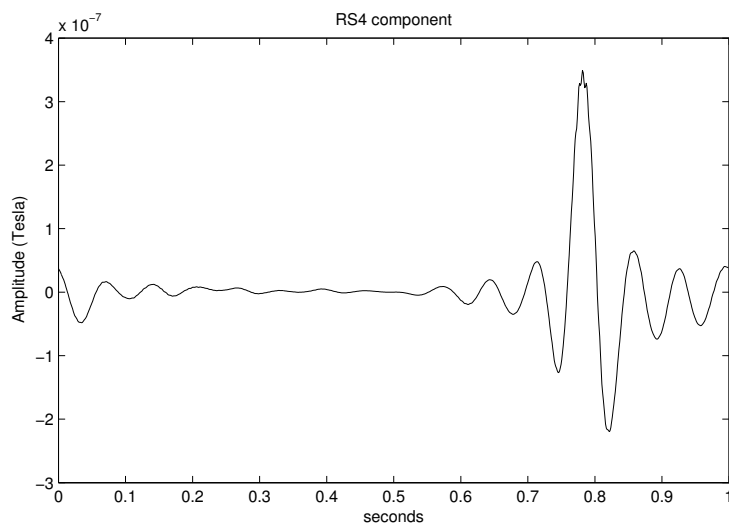


Figure 4-41. Resultant Spheric Caused due to the Return Stroke 4 of Current

Figure 4-42 shows the return stroke 5 of the current and Figure 4-43 shows the resultant sferic waveform.

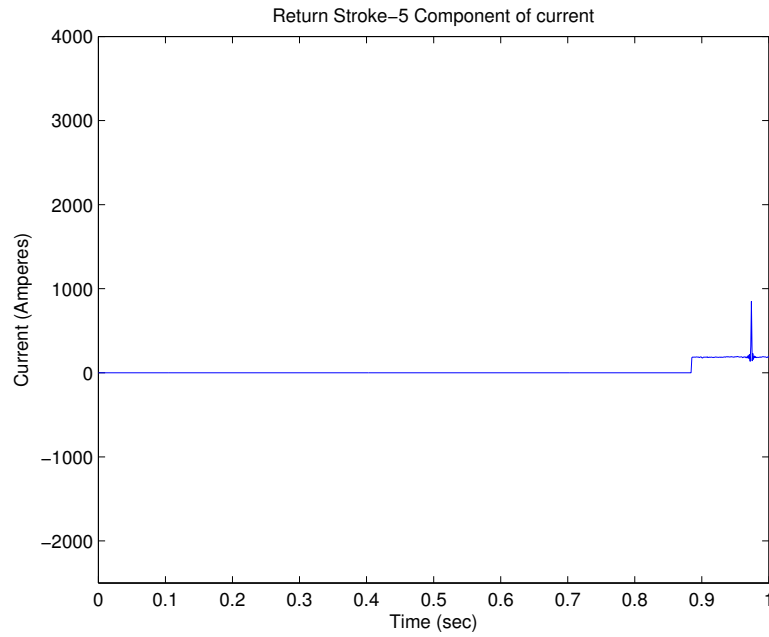


Figure 4-42. Return Stroke 5 of the Current Waveform Used

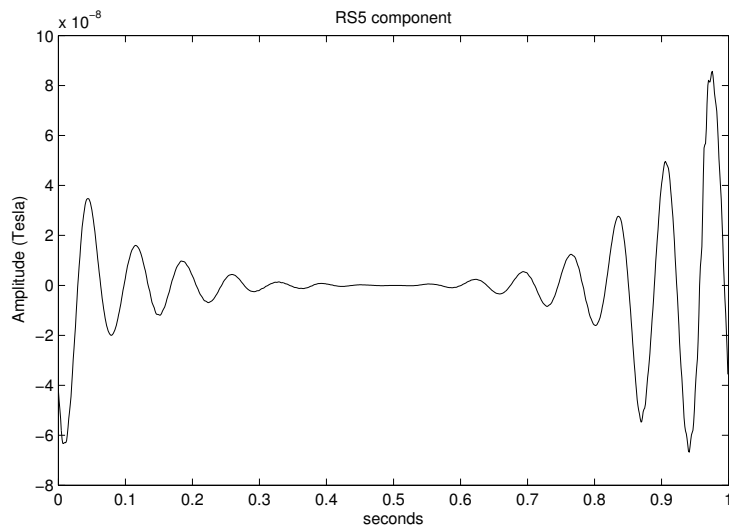


Figure 4-43. Resultant Sferic Caused due to the Return Stroke 5 of Current

#### 4.4.1 Effects of Current Components - Different Ionospheres

This section demonstrates the effects of the current components on the sferic waveforms under different ionospheres shown in the previous sections. In each of the following figures, the sferic waveform which results due to the entire current waveform is shown on which are overlaid the sferic waveforms due to each individual component. The sferic waveforms due to each individual component are overlaid only on the portion of the complete waveform where it has significant effect, the rest of the portion is clipped for a lucid view.

Figure 4-44 shows the sferic waveform with all the components laid out for the nighttime ionosphere with a valley.

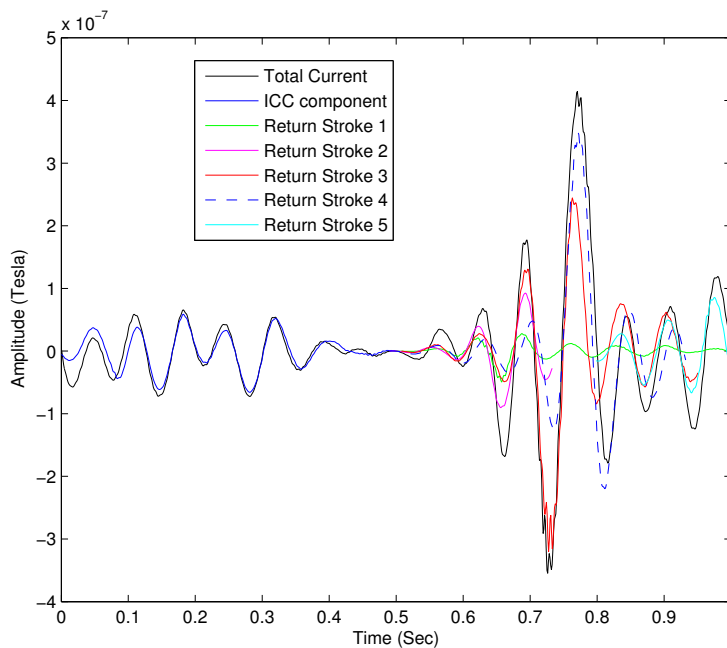


Figure 4-44. Sferic Waveform and Different Components-Nighttime Ionosphere With a valley

Figure 4-45 shows the sferic waveform with all the components laid out for the daytime ionosphere type 1.

Figure 4-46 shows the sferic waveform with all the components laid out for the nighttime ionosphere without a valley.

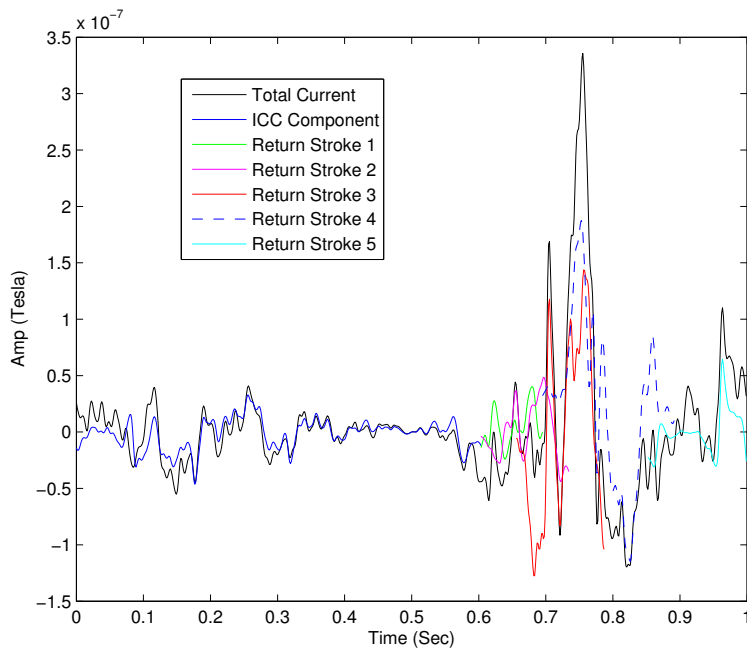


Figure 4-45. Spheric Waveform and Different Components-Daytime Ionosphere Type 1

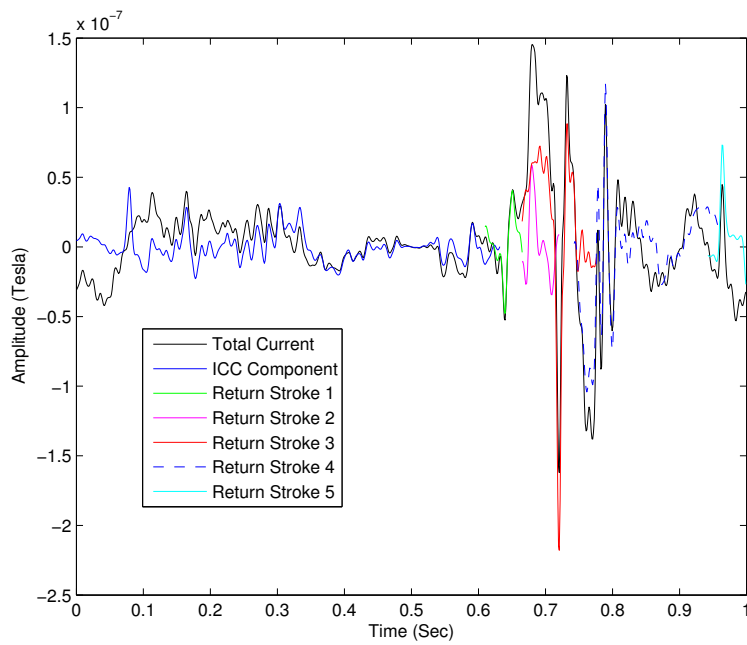


Figure 4-46. Spheric Waveform and Different Components-Daytime Ionosphere Without a valley

Figure 4-47 shows the sferic waveform with all the components laid out for the daytime ionosphere type 2.

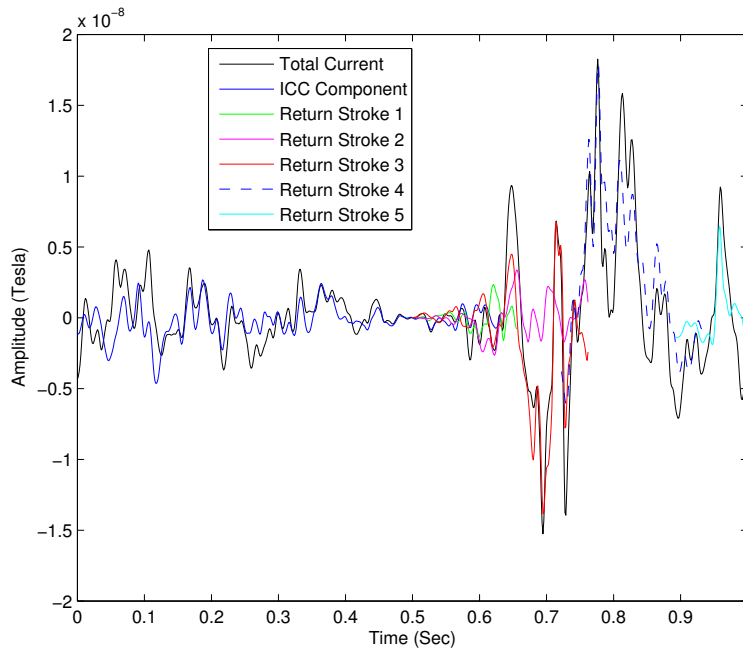


Figure 4-47. Sferic Waveform and Different Components-Daytime Ionosphere Type 2

It could be observed from the above figures that the ICC component does not have a significant effect on the sferic waveform, neither do return strokes one and two. Return Strokes three and four have the most significant effect on the waveform. Although the amplitude of return stroke 3 is much larger than return stroke 4 they have similar effect on the waveform, this is because of the continuous current in return stroke 4 which has greater impact on the sferic waveform.

## CHAPTER 5 SUMMARY AND SUGGESTIONS FOR FURTHER WORK

### 5.1 Summary

In this thesis the theoretical modeling of ELF radio atmospherics in the frequency range of 45-500Hz was carried on under different ionospheric conditions using a general theoretical formulation for the propagation of single frequency ELF/VLF signals in the Earth-Ionosphere waveguide developed by Budden ([Budden, 1961](#)) and implemented in a computer code ([Ferguson and C.H.Shellman, 1989](#)).

The path of propagation was taken from Camp Blanding, Florida to McMurdo Station in Antarctica. The modeling is done assuming a homogeneous ionosphere throughout the propagation path but a realistic ground conductivity profile with conductivity of the Earth's surface varying from  $10^{-3}$  to 4 S/m. The conductivity of land was varying from  $10^{-2}$  to  $10^{-3}$  depending on the geographic location, the conductivity of ice was  $10^{-4}$  and the conductivity of sea was taken as 4 S/m which are very realistic values. Different ionospheric profiles were used to study the dependence of propagation characteristics of the ELF waves on the ionosphere. It was observed that the amplitudes of the ELF waves were higher for the nighttime ionospheric conditions compared to daytime ionospheric conditions due to lesser electron density values of the nighttime ionosphere. For the nighttime ionosphere it was observed that the E-region of the ionosphere played an important role in determining the characteristics of the wave, especially the presence or absence of the valley at 100-150 km made a significant difference.

It was shown in the previous studies ([Cummer, 1997](#)) that the ELF sferics generated by a lightning are dependent on the current moment of the lightning. In this thesis the sferics generated due to rocket triggered lightning are considered and the actual current waveforms of rocket triggered lightning conducted at Camp Blanding, Florida are taken thereby providing a more realistic estimate of the characteristics of the sferics, unlike the

previous studies (Cummer, 1997) which have assumed a modeled impulsive lightning discharge.

## 5.2 Suggestions for Further Work

### 5.2.1 Jumps in the amplitude

When the amplitude of the spheric was plotted across the distance of propagation, it was observed that there were uneven jumps in the amplitude whenever there was a change in the conductivity of earth, the reason could not be explained and to rectify that the amplitudes were made smoother and continuous manually as demonstrated in Figure 5-1.

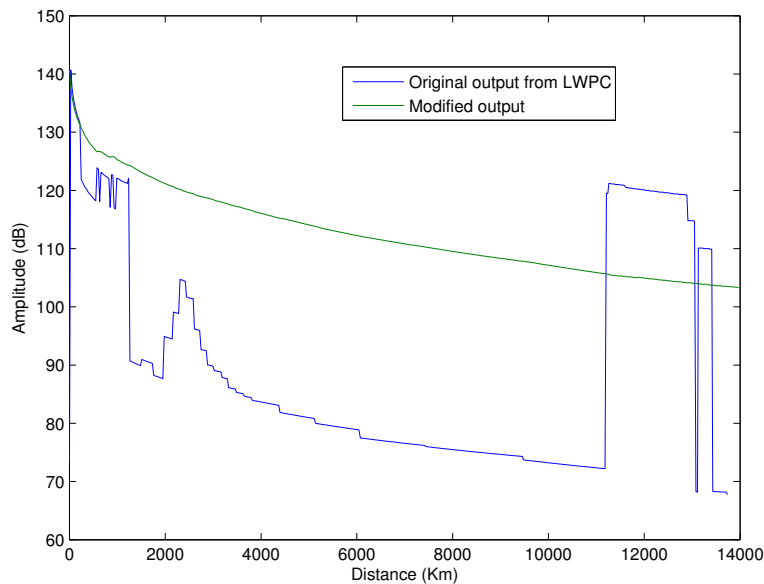


Figure 5-1. Variations in the amplitude of the spheric across the path of propagation

### 5.2.2 Modeling at Lower Frequencies - Below 45Hz

The lowest frequency that could be modeled in this thesis is 45Hz due to limitations of the MODEFNDR program. To get the MODEFNDR program to work in the ELF frequencies certain settings have to be changed to set it up to work in the iterative mode. In the iterative mode an initial guess for the Eigen angles is given and the program iterates on them to find the final solution within a specified range of tolerance. The

program finds the eigen angles that satisfy the mode condition in each horizontal slab and then couples each slab (a horizontal slab is a portion of the path where the waveguide parameters like the ground conductivity etc remain constant and whenever there is a change in any of the parameters beyond a specified limit a new slab is formed).

The MODEFNDR uses the same initial guess for every slab and there is a huge variation in certain waveguide parameters in the selected path of propagation and the eigen angles that satisfy the mode condition in one slab might not satisfy the mode condition in other. To model the sferics for this chosen path below 45 Hz this problem has to be rectified.

### **5.2.3 Modeling Using a more Realistic Inhomogeneous Ionosphere**

All the sferics presented in this thesis are modeled under the assumption of a homogeneous ionosphere throughout the propagation path. Although this is a reasonable assumption for smaller propagation distances, the distances considered in this thesis are long and the propagation path should include both the daytime and nighttime ionospheres. Moreover even for shorter distances a homogeneous ionosphere might not always reproduce some of the fine spectral details that could be seen in observed sferics (Cummer, 1997).

There are certain other effects like the presence of a strongly absorbing ionospheric inhomogeneities over a small area of the propagation path that have a strong effect on the sferic spectra and which cannot be modeled using a homogeneous ionosphere.

Also the FASTMC program ignores certain effects like the ionospheric variations transverse to the path of propagation and mode reflection which may result in the lack of certain spectral features in the modeled waveforms. Some of these problems could be rectified by using finite element or the finite difference methods.

#### 5.2.4 Remote Sensing of Ionosphere

Remote sensing of the ionosphere is a difficult problem due to its awkward height which is much lesser than the altitudes at which satellites are present and it is too high for the altitudes reached by balloons. Previously some methods were developed to remote sense the ionosphere using VLF and ELF sferics (Cummer, 1997) and (Cummer and Inan, 2000). The D-region of the ionosphere can be remote sensed using VLF sferics, but they cannot be used to remote the E-region of the ionosphere because they cannot penetrate the ionosphere beyond the D-region. However the ELF sferics have the capacity to penetrate this region due to their low attenuation rates, also their spectra are very sensitive to E-region electron densities as compared to the D-region. This makes them very suitable to remote sense the E-region of the ionosphere especially the presence of a valley in nighttime ionosphere in the E-region. The presence of the Sporadic-E layers also has a significant effect on the ELF sferic spectra. The Sporadic-E layer is not a common occurrence in the chosen propagation path and is a more common occurrence in the polar regions.

Sporadic E is the phenomenon of transient, irregularly scattered patches of relatively dense ionization that develop seasonally within the E-region of the ionosphere. This generally occurs at an altitude of 100-110 km and has a significant effect on the sferic propagation. In a theoretical study (Barr, 1977) showed that  $E_s$  generates a series of resonances from 10Hz to 1000Hz thereby having an effect on the attenuation rates. The frequencies and amplitudes of these resonances depend strongly on the characteristics of  $E_s$  layer.

A method has been previously developed (Cummer and Inan, 2000) to remote sense the E-region of the ionosphere and detect the presence of sporadic-E layers using ELF sferics, but this method assumes a single homogenous ground throughout the propagation path. By employing a similar method developed in (Cummer and Inan, 2000) and applying the procedure to the inhomogenous ground we can certainly

produce a much more realistic estimate, especially the effects of presence of sea in the path of propagation which has an important role to play in the attenuation rates.

## REFERENCES

- Barr, R. "The effect of sporadic-E on the nocturnal propagation of ELF radio waves." *Journal of Atmospheric and Terrestrial Physics* 39 (1977): 1379–1387.
- Bilitza, D. "International Reference Ionosphere 2000." *Radio Sci* 36 (2001): 261–275.
- Budden, K. G. *The wave-guide mode theory of wave propagation*. London: Logos Press, 1961.
- Burke, C. P. and D. L. Jones. "An experimental investigation of ELF attenuation rates in the Earth-ionosphere duct." *J. Atmos. Terr. Phys* 54 (1992): 243.
- Burton, E. T. and Boardman, E. M. "Audio-frequency atmospheric." *proc. IRE* 21 (1933): 1476.
- Crawford, D. E., Rakov, V. A., Uman, M. A., Schnetzer, G. H., Rambo, K. J., Stapleton, M. V., and Fisher, R. J. "The close lightning electromagnetic environment: Dart-leader electric field change versus distance." *J. Geophys. Res* 106(D14) (2001): 14,909–14,917.
- Cummer, S. A. *Lightning and Ionosphere Remote Sensing Using VLF/ELF Radio Atmospheric*. Ph.D. thesis, Stanford University, 1997.
- Cummer, S. A. and Inan, U. S. "Ionospheric E region remote sensing with ELF radio atmospheric." *Radio Sci* 35 (2000): 1437.
- Davies, K. *Ionospheric Radio*. London: Peregrinuss, 1990.
- Dermikol, M.K. *VLF Remote Sensing of the Ambient and Modified Lower Ionosphere*. Ph.D. thesis, Stanford University, 1999.
- D.Wang, Rakov, V. A., Uman, M. A., Fernandez, M. I., Rambo, K. J., Schnetzer, G. H., and Fisher, R. J. "Characterization of the initial stage of negative rocket-triggered lightning." *J. Geophys. Res* 104 (1999): 4213–4222.
- Dwyer, J. R., K., Rassoul H., Al-Dayeh, Caraway, M., B., L. Wright, A., Chrest, A., Uman M., A., Rakov V., J., Rambo K., M., Jordan D., J., Jerauld, and C., Smyth. "Measurements of x-ray emission from rocket-triggered lightning." *Geophys. Res. Lett.* 31 (2004).
- Evans, J. V. "Theory and practice of ionosphere study by Thomson scatter radar." *Proc. IEEE* 57 (1969): 496.
- Ferguson, J.A. F.P.Snyder D.G.Morfitt and C.H.Shellman. *Long Wave Propagation Capability Documentation*. Tech.Doc.1518. Naval Ocean Systems Center, 1989.
- Fioux, R. P., Gary, C. H., Hutzler, B. P., Eybert-Berard, A. R., Hubert, P. L., Meesters, A. C., Perroud, P. H., Hamelin, J. H., and Person, J. M. "Research on Artificially

- Triggered Lightning in France." *Power Apparatus and Systems, IEEE Transactions on PAS-97* (1978).3: 725–733.
- Hargreaves, J. K. *The Solar-Terrestrial Environment*. Cambridge: Cambridge University Press, 1992.
- Hauser, J.P W.E.Garner and F.J.Rhoads. *A VLF Effective Ground Conductivity Map of Canada and Greenland with Revisions from propagation data*. Report 6893. NRL, 1969.
- Hepburn, F. "Atmospheric waveforms with very low frequency components below 1 kc/s known as slowtails." *J. Atmos. Terr. Phys* 54 (1992): 243.
- Howard, J.S. *Lightning Propagation and Ground Attachment Process from Multiple Station Electric Field and X-RAY Measurements*. Ph.D. thesis, University of Florida, 2009.
- Inan, U.S. and A.S.Inan. *Electromagnetic Waves*. Prentice Hall, 1999.
- J.Jerauld, Rakov, V. A., Uman, M. A., Rambo, K. J., Jordan, D. M., Cummins, K. L., and Cramer, J. A. "An evaluation of the performance characteristics of the U.S. National Lightning Detection Network in Florida using rocket-triggered lightning." *J. Geophys. Res.* 110 (2005).
- Jones, D. L. "Extremely Low Frequency (ELF) ionospheric radio propagation studies using natural sources." *IEEE Trans. Comm.* 22 (1974): 477.
- Pappert, R. A. and Ferguson, J. A. "VLF/LF mode conversion model calculations for air to air transmissions in the earth-ionosphere waveguide." *Radio Sci* 21 (1986): 551–558.
- Prentice, S. A. and Mackerras, D. "The ratio of cloud to cloud-to-ground lightning ashes in thunderstorms." *Journal of Applied Meteorology* 16 (1977): 545.
- Rakov, R.A., Mata, C.T., Uman, M.A., Rambo, K.J., and Mata, A.G. "Review of triggered-lightning experiments at the ICLRT at Camp Blanding, Florida." *Power Tech Conference Proceedings, 2003 IEEE Bologna*. vol. 3. 2003, 8 pp. Vol.3–.
- Rakov, V. A. and Uman, M. A. *Lightning Physics and Effects*. Cambridge: Cambridge University Press, 2003.
- Reising, S. C., Inan, U. S., Bell, T. F., and Lyons, W. A. "Evidence for continuing current in sprite-producing cloud-to-ground lightning." *Geophys. Res. Lett.* 23 (1996): 3639.
- Richter, J. H. "Application of Conformal Mapping to earth flattening procedures in radio propagation problems." *Radio Sci* 1 (1966): 1435.

- S.A.Cummer and U.S.Inan. "Modeling ELF radio atmospheric propagation and extracting lightning currents from ELF observations." *Radio Science* 35 (2000): 385–394.
- Taylor, W. L. and Sao, K. "ELF attenuation rates and phase velocities observed from slow-tail components of atmospherics." *Radio Sci* 5 (1970): 1453–1460.
- Uman, M. A. *The Lightning Discharge*. orlando: Academic Press, 1987.
- Wait, J. R. *Electromagnetic Waves in Stratified Media*. Oxford: Pergamon Press, 1970.
- Weidman, C. D. and E. P. Krider. "The amplitude spectra of lightning radiation fields in the interval from 1 to 20 MHz." *Radio Sci* 21 (1986): 964.
- Wood, T. G. *Geo-Location of Individual Lightning Discharges using Impulsive VLF Electromagnetic Waveforms*. Ph.D. thesis, Stanford University, 2004.

## BIOGRAPHICAL SKETCH

Bharat Kunduri was born in Hyderabad, India in 1987. He graduated with a bachelor's degree (Honor's) in electrical and electronics engineering from Dr.M.G.R.University, Chennai, India in 2008. He pursued his master's degree at University of Florida under the guidance of Dr. Robert Moore. His research interests lie in the field of electromagnetics and study of Ionosphere.